

**FROM DEVELOPMENTAL BIOLOGY TO TISSUE-ENGINEERING:
PRINTING BLOOD VESSELS**

A Dissertation
presented to
the Faculty of the Graduate School
at the University of Missouri-Columbia

In Partial Fulfillment
of the Requirements for the Degree
Doctor of Philosophy

by
CYRILLE NOROTTE
Dr. Gabor Forgacs, Dissertation Supervisor

MAY 2009

The undersigned, appointed by the dean of the Graduate School, have examined the dissertation entitled

FROM DEVELOPMENTAL BIOLOGY TO TISSUE-ENGINEERING:

PRINTING BLOOD VESSELS

presented by Cyrille Norotte,

a candidate for the degree of doctor of philosophy of Biological Sciences,

and hereby certify that, in their opinion, it is worthy of acceptance.

Professor Gabor Forgacs

Professor Anand Chandrasekhar

Professor Ioan Kosztin

Professor David Worcester

A mes grands-pères

ACKNOWLEDGEMENTS

I first would like to thank my advisor, Gabor Forgacs. His enthusiasm has been highly “contagious”. He has created a truly interdisciplinary research environment that made me navigate between biology, physics, and engineering throughout my research time in his lab; a fact that I deeply enjoyed, coming from a more biological background. I enjoyed his insight and patience in the passionate discussions that we have had over the last few years. I also appreciate the freedom he gave me in conducting my research projects while being always available for help in every respect. Finally, I would like to thank him for giving me a confidence and experience that are inestimable, and will be very useful in the future.

Second, I would like to thank Francoise Marga without whom this work would have never been achieved. She has trained me and collaborated with me on many aspects of the research presented here. I am really grateful for her time, patience and her meticulous guidance throughout these years. I have also been fortunate to be surrounded by my other colleagues and close collaborators Mingzhai Sun, Catalin Staiculescu, Gabi Hosu, Zhongkui Hong, Brook Damon, Karoly Jakab, Bogdan Barz, Adrian Neagu, Lorant Janosi, Elijah Flenner and Jhuma Das. I have strongly benefited from their multi-disciplinary backgrounds throughout discussions and collaborations on various research projects, and from the friendship and basketball skills of many of them.

I would like to express my gratitude to Dr. Ioan Kosztin. His advice and contributions to this work have been invaluable. I have strongly benefited from his superb

physical and mathematical background, coupled with his kindness and enthusiasm. I also would like to deeply thank my French mentor, Francois Amblard from Institut Curie in Paris, who has always been available and with whom I have also shared passionate discussions. He has strongly contributed to my intellectual upbringing in biophysics.

I also thank Dr. Laura Niklason from Yale University who has welcomed me in her lab and shared her experience on vascular tissue-engineering and bioreactor systems. Special thanks to Dr. Stuart Newman from New-York Medical College for the many insightful discussions. His knowledge of developmental biology and evolution has been inestimable. I would like to acknowledge my other committee members Dr. Anand Chandrasekhar and Dr. David Worcester for their advice and time.

I am incredibly grateful to Sam Potts and Roderick Schlotzhauer from the Machine Shop of the Physics department, who helped designing and building all the specific pieces of equipment used in this work. Deep thanks to Nila Emerich from the Department of Biological Sciences. Her kindness and support have guided me through these years. Thanks also to Jill Gruenkemeyer and Jan Adair from the RADIL histology core, and Marilyn Beissenherz from the Veterinary Department for their assistance.

TABLE OF CONTENTS

ACKNOWLEDGEMENTS	ii
LIST OF FIGURES	vii
LIST OF TABLES	ix
ABSTRACT.....	x
CHAPTER I: INTRODUCTION	1
Developmental Biology and Regenerative Medicine	1
Physical mechanisms in morphogenesis.....	5
Tissue-liquidity based tissue-engineering	9
Rationale for vascular tissue-engineering.....	11
The vascular wall: a model for surface-tension based tissue patterning.....	11
Implications of vascular tissue-engineering.....	12
CHAPTER II: HYPOTHESIS AND SPECIFIC AIMS.....	15
Central hypothesis	15
Specific aim 1	15
Specific aim 2	15
Specific aim 3	16
Specific aim 4	16
Specific aim 5	16
CHAPTER III: MATERIALS AND METHODS.....	17
General Cell Culture Procedures	17
Cell Source and Culture	17

Chinese Hamster Ovary Cells.....	17
Human Umbilical Vein Smooth Muscle Cells.....	17
Porcine Aortic Smooth Muscle Cells.....	18
Human Umbilical Vein Endothelial Cells	18
Human Skin Fibroblasts.....	19
Cryopreservation	19
Microtissue fabrication.....	20
Multicellular spheroids preparation	20
Cushion Tissue Spheroids Preparation	21
Multicellular cylinder preparation	21
Measurement of liquid interfacial tension and apparent tissue surface tension	22
Segregation assays.....	25
Cell-sorting assay.....	25
Tissue-envelopment assay	25
Macrotissue fabrication.....	26
Maturation of engineered vascular constructs.....	28
Microscopy.....	30
Histological and immunohistochemical analysis.....	30
Cell Viability and Proliferation.....	31
Visualization of cell-segregation patterns.....	31
Scanning Electron Microscopy of multicellular spheroids surface	32
CHAPTER IV: “LIQUID-LIKE” PHENOMENA GOVERN SELF-ASSEMBLY OF VASCULAR CELLS INTO MICROTISSUE <i>IN VITRO</i>	33
Introduction.....	33
Surface tension: theoretical considerations	34

Formulation of the mathematical problem for the relevant experimental conditions	34
Exact solution of the Laplace equation: the surface tension in terms of experimentally measurable quantities.....	36
Generalization to simultaneous compression of several droplets	39
Incompressibility.....	39
Interfacial and surface tension measurement of liquids, tissues, and multicellular spheroids	41
Surface tension guides the self-assembly of vascular cells <i>in vitro</i>	47
CHAPTER V: DIRECTING MICROTISSUE SELF-ASSEMBLY TOWARDS COMPLEX MACROVASCULAR STRUCTURES	54
Introduction.....	54
Building scaffold-free, customized macrovascular tubular structures using multicellular spheroids	57
Using multicellular cylinders as building-blocks for vascular tissue-engineering.....	61
Bioprinting of single and double-layered vascular tubes	62
CHAPTER VI: CONCLUSIONS AND PERSPECTIVES.....	66
Specific aim 1	66
Specific aim 2	69
Specific aim 3	70
Specific aim 4	72
Specific aim 5	76
Current and future directions: Maturation of tissue-engineered vessels	77
REFERENCES.....	81
VITA.....	92

LIST OF FIGURES

Figure	Page
1. Apparent liquid-like properties of embryonic tissues	7
2. Multicellular cylinder preparation.....	22
3. Parallel plate compression device for surface tensiometry	24
4. Manual and computer-aided tissue assembly system.....	27
5. Perfusion bioreactor	29
6. Schematic diagram of an uncompressed and compressed liquid drop at shape equilibrium	35
7. Plot of $f_{\theta}(\alpha)$, and $\beta_{\theta}(\alpha)$ for different values of the contact angle θ	38
8. Compression of liquid droplets and tissue spheroids	42
9. Employing eq. (7) for data evaluation.....	43
10. Scanning electron micrographs of multicellular spheroids	45
11. Testing incompressibility	47
12. Liquid-like segregation of multicellular spheroids	48
13. Results of cell segregation assays	50
14. Time-course of envelopment and cell sorting assays.....	52
15. Illustration of how self- and cross-adhesions determine the most stable equilibrium configuration.....	53
16. Organ printing concept.....	55
17. Patterns used for engineering custom-shaped tubular structures	57
18. Fusion pattern of various multicellular spheroids assembled into tubular structures.....	59
19. Assembly of a hierarchical vascular tree.....	61

20. Bioprinting of multicellular cylinders into simple tubular patterns	63
21. Building a double-layered vascular wall	64
22. Histological analysis of matured PASMC constructs	79

LIST OF TABLES

Table	Page
1. Interfacial and surface tensions of liquids, tissue and multicellular spheroids	44

ABSTRACT

Cardiovascular disease is a leading cause of death and often requires vascular reconstruction. However, the use of synthetic materials and scaffold-based approaches has shown several limitations for small-diameter blood vessel tissue-engineering, evidenced by the fact that they can elicit adverse host responses and interfere with, rather than guide, direct cell-cell interaction as well as assembly and alignment of cell-produced extracellular matrix. Understanding the physical principles of biological self-assembly is thus essential for developing efficient strategies to build living tissues and organs. Here we exploit well-established liquid-like developmental processes (such as tissue fusion, envelopment or cell-sorting phenomena) to engineer scaffold-free, multilayered, small-diameter blood vessels. In particular, we show that apparent surface tensions of the three major vascular cell types (endothelial cells, smooth muscle cells and fibroblasts), determined through the exact solution of Laplace equation, guide their segregation in a multilayered fashion *in vitro*. Moreover, we introduce a novel rapid-prototyping technology (bioprinting) that allows for directing the self-assembly of the vascular cell types into custom-shaped tubular tissue structures, from single vascular tubes to complex hierarchical macrovascular trees. In addition to its potential for fulfilling the crucial need for small diameter vascular grafts and providing new strategies for vascularization of tissues for transplantation, this physically based approach provides a new insight into cell-patterning and structure formation and questions the paradigm of scaffold-based tissue-engineering.

CHAPTER I: INTRODUCTION

Developmental Biology and Regenerative Medicine

The understanding of developmental mechanisms involved in organ formation comes with the expectation that they could eventually be repeated or mimicked in order to regenerate or engineer new tissues and organs. This proposition holds partially true and is characterized by the parallel development of two principal strategic approaches to regenerative medicine, both closely related to developmental aspects of organ formation. The first approach intends to control cell fate while the second deals with the creation of structure and shape.

Contrary to the spectacular ability of some species such as amphibians urodeles that can regenerate limbs amputated at any level of the proximo-distal axis [1], mammals have a limited regenerative potential, with exceptions of a few tissues such as liver, epidermis, or blood. Natural regeneration involves cell plasticity at various cellular levels from stem cells to fully differentiated cells, and, depending on the species and the tissue of interest, processes such as proliferation, dedifferentiation, transdifferentiation, or differentiation, [2]. Promising progress has been achieved over the past years in the identification of embryonic and adult cell populations capable of contributing to the regeneration of multiple tissues and organs [3], in providing methods to direct the differentiation of embryonic or adult stem cells into desirable cell lineages [4, 5], and

even recently in the ability to dedifferentiate human adult cells into ES-like pluripotent cells [6, 7].

Despite these advances, it is now clear that the therapeutic success of cell-based approaches is strongly limited by the difficult task of guiding tissue assembly from these cells *in vivo*. Indeed the idea that, similarly to limb regeneration in urodeles, stem cells or differentiated cells, after introduction at the lesion site, would directly participate in the building of the tissue has fallen short of expectations. Poor engraftment, large-scale cell death, or loss of control over the fate of introduced cell populations have been major hurdles, although it is true that successfully integrated cells can contribute, directly or indirectly, to the repair of damaged or diseased tissue [8]. The limited control over the local environment *in vivo* has contributed to the development of more realistic *ex-vivo* approaches to guide tissue formation. Tissue-engineering has emerged as an interdisciplinary field that applies the principles of engineering and the life sciences toward the development of tissue substitutes for regeneration, repair, or replacement of damaged or diseased tissues [9, 10]. How closely should tissue-engineers try to imitate developmental morphogenesis in order to capture the most essential structure-function features of normal human tissues is still an open question. It is already clear that tissue-engineering has integrated developmental biology in a “biomimetic” approach that intends to provide the biological, chemical, and mechanical clues to guide eventual cell differentiation and assembly into a 3D tissue construct with a real-time insight [11, 12]. Methods to control the microenvironment *in vitro* include seeding cells on scaffold materials (native or synthetic, permanent or biodegradable) to provide an analog of the

extracellular matrix, growing and maturing engineered tissues in bioreactors, or directing cell fate using soluble clues (e.g. morphogens) or by genetic manipulation [13, 14].

3D structure formation in classical tissue-engineering is achieved by the use of scaffolds, dominating conceptual paradigm. Scaffolds provide a three-dimensional environment for cell attachment and growth [15, 16]. Indeed it is widely accepted that using scaffolds of predetermined size and shape represents the best way to control the final geometry of tissue-engineered constructs as illustrated by the infamous “ear on a mouse” [17]. This approach has led to significant results in the reconstruction of various tissues and organs including skin, bone, cartilage, meniscus, bladder, and has, in some cases, been further translated to clinical practice [18-22].

Classical scaffold-based approaches still face general as well as specific challenges. Scaffold choice, immunogenicity, degradation rate, toxicity of degradation products, host inflammatory responses, mechanical mismatch with surrounding host tissue are key issues, that may affect the long term behavior of the tissue-engineered transplant [23]. Some of the shortcomings cited above can directly interfere with the primary function of the engineered tissue. An example is myocardial tissue that presents high cell density necessary to assure synchronous beating through gap junctions that tightly interconnect neighboring cells. However, the use of scaffolds for cardiac tissue-engineering has been associated with reduced cell-to-cell connection as well as incorrect deposition and alignment of extracellular matrix (ECM), affecting scaffold biodegradation and the force-generating ability of myocardial constructs [24, 25]. Problems associated with the production and alignment of ECM (i.e. collagen and elastin) especially are critical in vascular tissue engineering. Largely for this reason the promise

of a small-diameter blood vessel substitute with mechanical strength comparable to that of native vessels for adult arterial revascularization, often described as the “holy grail” of tissue-engineering, remains unrealized. In addition to the recurrent difficulty to produce elastic fibers *in vitro* [26], the use of scaffolds in conjunction with cells has raised several challenges: the inherent weakness of collagen gels hinders the final strength of the tissue-engineered vessel [27], or the presence of residual polymer fragments can disrupt the normal organization of the vascular wall [28, 29] and even influence smooth muscle cell phenotype [30]. Therefore it is not surprising that the first clinical applications of tissue-engineered vascular grafts have either targeted low-pressure applications [31] or have been accomplished by using an entirely scaffold-free method termed sheet-based tissue-engineering [32, 33] (currently under study for myocardial reconstruction as well [34]).

Despite the few promising attempts, it is clear that, due to the dominant use of scaffolds, natural three-dimensional self-assembly properties of cells utilized in morphogenetic processes and pattern formation during embryonic development have had little influence in tissue-engineering strategies so far. While developmental processes are widely recognized to be mediated by a pool of evolutionary conserved genes, the relationship between these molecular determinants and the physics underlying these processes has been generally ignored. In the next paragraph, we show that physical mechanisms and particularly those associated with the theory of liquids, are essential in understanding some morphogenetic aspects of embryonic development and can provide a framework for a novel tissue-engineering strategies.

Physical mechanisms in morphogenesis

Even though the genetic background of many developmental processes has been extensively studied, it is clear that gene products act in a specific physical context that guides shape and pattern formation within defined environmental limits throughout evolution [35]. Physical mechanisms driving embryonic development include adhesion, diffusion, oscillation, anisotropy or lateral inhibition and are involved in various transformations such as tissue multilayering, elongation of multicellular mass, segmentation, formation of internal cavities, or induction of alternative cell types [36].

One interesting property of embryonic tissues comes from the observation that, on a time scale of hours, they behave analogously to highly viscous, incompressible liquids [37-40]. Phenomena such as the spreading of one liquid over the surface of another and the "breaking" of a dispersion or emulsion of two immiscible liquids have found their biological equivalents such as tissue spreading, fusion or cell-sorting which contribute to the establishment and maintenance of boundaries and compartments during morphogenesis [41, 42] (Figure 1). This analogy allowed for the description of well-known developmental processes such as gastrulation [43] and limb budding [44, 45]. Another example concerns the spontaneous rounding-up of irregular tissue fragments or cell aggregates *in vitro* similar to the perfectly spherical shape assumed by a liquid droplet in absence of external forces (e.g. gravity). Indeed a liquid drop minimizes its interfacial area with the surroundings in order to achieve a state of minimal surface or interfacial energy. This surface or interfacial energy per unit area of is called surface or interfacial tension and is denoted by σ . Thus, the energy cost to increase the surface of a

liquid by a unit area is given by the liquid's surface tension. Strictly speaking, the term "surface tension" is reserved for the case where the liquid is surrounded by air, while "interfacial tension" is used when the liquid is in contact with another liquid or a solid phase. The surface tension of a liquid characterizes the tendency of its global surface area to decrease. Another way to look at the spherical drop shape is by considering that liquid molecules are mutually attracted by various intermolecular forces (Van der Waals forces, ionic interactions, hydrogen bonds) [46], but yet move in order to seek positions of maximal binding (i.e. each molecule is completely surrounded by other liquid molecules), with the consequence that the surface area of the liquid drop becomes minimal. The spherical shape is thus the outcome of maximal binding between liquid molecules and thus corresponds to the state of lowest surface energy, as mentioned earlier. It is then easy to understand why immiscible liquids such as oil and water, when mixed together, undergo phase separation: the less cohesive liquid surrounds the more cohesive one (oil has a lower surface tension than water) in order to minimize the overall interfacial and surface energy of the system. In summary, a liquid system is composed of subunits which are mobile and cohesive at the same time.

By analogy with immiscible liquids, Steinberg proposed that rearrangements of mobile cells during embryonic tissue segregation, mutual envelopment or sorting were guided by differences in intercellular adhesion [47-51]. This suggestion was later formulated as the Differential Adhesion Hypothesis (DAH) [52] and accounted for earlier observations in amphibian embryonic tissues by Holtfreter referred to as "tissue affinities" [53, 54].

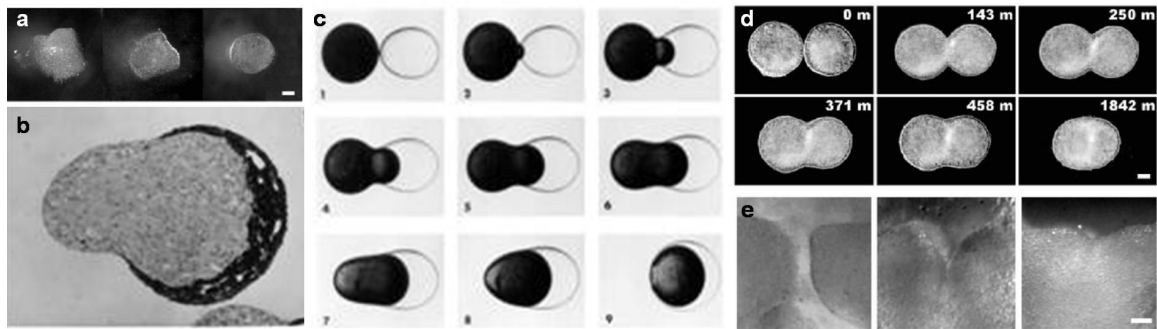


Figure 1. Apparent liquid-like properties of embryonic tissues. (a) An irregular cushion tissue fragment, excised from 5-day (Hamburger and Hamilton [HH] stage 27) chick embryo rounds up into a spheroid in approximately 24 hr. (b) The mutual envelopment behavior of distinct embryonic tissues closely resembles the coalescence of immiscible liquids (c): a water droplet being progressively surrounded by an oil droplet (d) Two contiguous spheroids in culture medium fuse in time (indicated in minutes), similarly to liquid drops. (e) *In vivo* cushion tissue fusion during chicken heart development. Panels from left (4.5 day, HH stage 26 embryo) to right (day 5.5, HH stage 28) show the gradual blending of the two atrioventricular cushion tissues. Scale bars 100 μm . Adapted from [55-58]

The introduction of tissue surface tensiometry [59] further validated the liquid analogy and confirmed surface-tension based predictions concerning the mutual envelopment and sorting behavior of embryonic tissues. Indeed, similarly to any liquid tending to spread over any other liquid of greater surface tension, the equilibrium configurations arrived at after a group of tissue samples are combined in all possible pairs revealed the operation of a strict rule of transitivity, the tissue of greatest cohesivity (highest surface tension) tending to be spread upon by all of the others [60]. For precision, tissue surface tension or the “apparent” surface tension of a tissue denotes in fact the interfacial tension between a tissue and the surrounding culture medium in which its measurement is performed [59]. Despite these analogies, it has to be emphasized that

tissues are not liquids. The movement of loosely bound liquid particles is driven by van der Waals forces and powered by thermal energy with scale set by kT (k —Boltzmann constant, T —absolute temperature). On the other hand the motion of cells bound in tissues by cell adhesion molecules or substrate adhesion molecules is powered by metabolic energy, with scale set by ATP hydrolysis. Apparent tissue surface tension however provides a useful means to systematically interpret equilibrium cellular arrangements and distinguish between tissues containing motile and adhesive cells. In support of the DAH, it was shown that binding specificity or differences in expression levels of adhesion molecules such as cadherins were sufficient to drive cell segregation *in vitro* [61, 62] and *in vivo* [63] and more recently, that tissue surface tension increased linearly with the expression level of cadherins at the cell surface [64]. Yet, it should be emphasized that alternative hypotheses explaining tissue segregation have been formulated: according to the “differential surface contraction hypothesis”, tissue surface tensions were derived from contractile forces associated with surface regions (cortex) of individual cells rather than from their intercellular binding strengths [65, 66]. This hypothesis, which suffered earlier from the lack of appropriate methods to measure or modify cortical tension, has been recently revisited both experimentally and through computational simulations [67, 68], showing that both cortical tension and intercellular adhesion may contribute positively to tissue surface tension and influence tissue segregation, thus reconciling the two hypotheses. In the present work, we do not intend to decipher the mechanisms contributing to tissue surface tension, but rather to use the physical properties of tissues as a conceptual framework for pattern and shape formation in a tissue-engineering perspective.

Tissue-liquidity based tissue-engineering

The aforementioned physical context underlying the self-assembling and self-organizing properties of embryonic tissues can be used as a conceptual framework for *in vitro* tissue assembly from single cells without the use of any scaffold. For this purpose, two levels of structure and pattern formation are equally important: the first level concerns the formation of 3D microtissues from single cells while the second relates to the assembly of these microtissues as subunits into more complex macrotissue structures.

It has been long recognized that tissue micro-spheres (usually less than a millimeter in diameter) could be reconstructed *in vitro* from dissociated cells [50, 69-73]. More recently, a wide range of techniques such as hanging drops cultures or micromolding [74] have been developed by different research groups including ours for the production of 3D size-specific multicellular spheroids from 2D cultures [75, 76]. Interest in multicellular spheroids for biomedical and tumor research [75, 77-80] has stemmed from the fact that, in many aspects, they exhibit higher similarity to real tissues compared to monolayer cultures, for example, in terms of extracellular matrix production [81] or functional capabilities [82]. In tissue-engineering applications, they have served as 3D models for liver [83], pancreas [84], blood vessel [85, 86], myocardial muscle [87], ganglion [87] or bone reconstruction [88]. Liquid-like phenomena already play an important role at micro-level, illustrated by the natural rounding-up of multicellular aggregates, or by cell-segregation when mixtures of different cell types contribute to the formation of a single spheroid [89, 90]. As it will be demonstrated, the liquid properties of rounded tissues, which can be evaluated by tissue tensiometry [59, 91], will guide our engineering

strategy not only at the microtissue level, but also at a more global scale when multicellular spheroids self-organize into larger tissue structures. This will be accomplished by recapitulating tissue fusion, a major morphogenetic process during embryonic development, in vitro [92]. We have recently shown, through experimental and computational studies, that tissue fusion (illustrated in Fig. 1) can be quantified by the same theoretical analysis that applies to the fusion of true liquid drops [40, 56]. Taking advantage of tissue fusion, it was shown that macro-tissues of defined shapes such as rings, square sheets or cylinders could be generated through the fusion of multicellular spheroids within permissive hydrogels such as collagen [93-95] or on adhesion-free gels like agarose [96, 97]. Despite these advances precision and reproducibility through manual deposition of micro-tissues remain challenging.

To better guide tissue self-assembly at the macroscale level, a novel technology, “Organ printing” was introduced with the idea that a rapid prototyping method would enable reproducible, scalable, mass production of tissue-engineered products [98, 99]. This technology is based on the conceptual framework that “bioink” particles (i.e. multicellular spheroids) can be “printed” on a “biopaper” (i.e. permissive hydrogel) in a repeated fashion, layer-by-layer, in order to build a 3D structure. Experimentally, this method allowed for the precise deposition of multicellular spheroids into collagen gels, followed by a post-processing phase where spheroids fused to form macro-tissues of prescribed shape, such as tubes or sheets [55, 94]. One of the main limitations of this method is the use of hydrogels as a support for spheroid fusion. First, it is reasonable to assume that part of the gel is incorporated in the final tissue structure, as spheroids fuse together through the gel. Thus, this method is not completely scaffold-free. Second, it is

challenging to separate the gel (especially collagen) from the final tissue once the structure has formed. It should be emphasized that other “printing” methods have been applied in the tissue-engineering field: interestingly, most of them have concentrated on scaffold fabrication [100], while few have attempted to tackle the challenge of printing living cells [101, 102].

Rationale for vascular tissue-engineering

Although the aforementioned biophysical (liquid-like properties of tissues) and technological (bioprinting) framework could be used for engineering a large range of different tissues, the present work concentrates mostly on vascular tissue-engineering, for two main reasons. The first relates to the possibility of using tissue-liquidity for cell patterning, as the vascular wall is composed of three different cell types segregated in a multilayered fashion, while the second relates to the implications of vascular tissue engineering for regenerative medicine.

The vascular wall: a model for surface-tension based tissue patterning

A native blood vessel is typically composed of three different structural layers containing distinct cell populations. The innermost layer is the tunica intima composed of a monolayer of endothelial cells. The middle layer is the tunica media and displays concentric layers of smooth muscle cells. Finally, the outer layer, or tunica adventitia, is composed of loosely arranged fibroblasts. To our knowledge, this multilayered

segregation of distinct cell populations within the vascular wall has never been studied biophysically. Previous studies have clearly demonstrated that these vascular cell types have the ability to sort or mix *in vitro* 3D co-culture models under certain environmental factors (such as VEGF induction) although the reported final configurations are sometimes contradictory [74, 86, 89, 103, 104], and difficult to quantitatively interpret. As mentioned earlier, tissue tensiometry is a useful tool for understanding tissue segregation phenomena, and has extensively been applied to a number of tissues, including the pancreas [90]. Therefore, in the present work, we use tissue tensiometry to measure the relative cohesivities of the three vascular cell types and see how these cohesivities relate to the segregation of these cells *in vitro*. To our knowledge, building a complete vascular wall through self-assembly has not been achieved, and is a difficult task even within scaffold-based tissue engineering [29].

Implications of vascular tissue-engineering

The most important short-term goal of vascular tissue-engineering relates to the immediate and critical need of a small-diameter blood vessel substitute for cardiovascular surgery. Indeed, cardiovascular disease is the leading cause of death in the western world and often requires vascular reconstruction. Synthetic materials such as expanded polytetrafluoroethylene (ePTFE) and Dacron have been used with great success for bypass conduits greater than 6 mm in diameter, but when used in the coronary system, where diameters are 3–4 mm, thrombotic events rapidly close them off [105, 106]. In the United States alone, about half a million of coronary artery bypass graft surgeries are

performed annually [107]. The gold standard for this procedure is the use of autologous vessels, commonly either the patient's internal mammary artery or the saphenous vein. However, suitable vein or artery tissue is not always available for peripheral or coronary revascularization, because of previous vessel harvesting or disease. And even when appropriate native vessels are available, removing them from their normal positions in the vasculature is less than desirable. The need for alternatives to native blood vessels necessitates the urgent engineering of a small-diameter blood vessel substitute with patency equivalent to that of native tissue [108], the Holy Grail of tissue engineering, at present. There has been extensive research over the last 20 years on the use of scaffold materials in conjunction with cells for small-diameter blood vessel reconstruction. Although acute thrombogenic issues have been solved by adding a functional endothelium to the grafts' lumen, current grafts are still inferior to autologous vessels, especially on the long term, mainly because of anastomotic intimal hyperplasia, and eventually atherosclerosis, resulting from the mechanical mismatch between the implanted conduit and the connecting vasculature [109]. As mentioned earlier, there are additional general problems associated with scaffolds, such as degradation rate, toxicity of degradation products or host inflammatory responses due to the presence of residual scaffold-polymer fragments. Such fragments may disrupt the normal organization of the vascular wall [28, 29] and even influence smooth muscle cell (SMC) phenotype [30]. We believe a self-assembly approach to vascular tissue-engineering, such as the one presented in this work, could solve many of the afore-mentioned scaffold-related issues.

In addition to its immediate relevance to bypass surgery, vascular tissue-engineering has long-term implications as it holds the promise to revolutionize the entire

tissue-engineering field. This is related to most critical and still unsolved problem in tissue-engineering, the vascularization of thick tissue constructs [110, 111]. This is absolutely necessary as diffusion of nutrients and oxygen in tissues is limited to a few hundred microns *in vitro* [112]. Even though the engineering of microvascular (but not macrovascular) networks *in vitro* has recently been reported (leading to the production of prevascularized bioengineered tissues [113-116]),, viability of such tissues upon implantation still remains problematic. This is primarily due to the fact that infiltration of surrounding vessels or connection of microvascularized constructs with the host vasculature takes several days potentially predisposing the tissue to ischemia [111]. A method to build hierarchical macro- to micro-vascular trees would represent significant progress towards the vascularization of thicker tissues. This would allow the engineered tissue to be perfused for maintenance and maturation *in vitro* before being surgically connected to the host macrovasculature (as it is commonly done for whole organ transplants). In the present work, we introduce a method, to our knowledge the first, that allows to build hierarchical macro-vascular trees.

CHAPTER II: HYPOTHESIS AND SPECIFIC AIMS

Central hypothesis

Complex, multilayered, scaffold-free vascular tubular structures can be engineered through the self-assembly of vascular cells activated by innovative technologies (i.e. bioprinting) and guided by physical principles (i.e. associated with tissue liquidity) .

To address the central hypothesis, five specific aims were defined.

Specific aim 1

Evaluate the liquid behavior of multicellular spheroids composed of any of three vascular cell types (endothelial cells, smooth muscle cells and fibroblasts) and determine their relative cohesivities by tensiometry.

Specific aim 2

Study the segregation of the three vascular cell types in tissue spreading or cell-sorting assays in light of their relative cohesivities.

Aims 1 and 2 are addressed in Chapter IV.

Specific aim 3

Combine tissue segregation and tissue fusion processes to create a multilayered vascular wall containing the three vascular cell types in a pattern similar to that in native vessels.

Specific aim 4

Develop a scaffold-free approach for guiding the self-assembly of multicellular vascular spheroids into custom-shaped macrovascular structures.

Specific aim 5

Adapt the aforementioned approach to a rapid prototyping technique, i.e. bioprinting.

Aims 3, 4 and 5 are addressed in Chapter V.

CHAPTER III: MATERIALS AND METHODS

General Cell Culture Procedures

Cell Source and Culture

Chinese Hamster Ovary Cells

Chinese Hamster Ovary (CHO) cells transfected with N-cadherin (courtesy of A. Bershadsky, Weizmann Institute, Rehovot, Israel) were grown at 37°C with 5% CO₂ in Dulbecco's Modified Eagle Medium (DMEM; Gibco/Invitrogen, CA) supplemented with 10% Fetal Bovine Serum (Atlanta Biologicals, GA), antibiotics (100U/mL penicillin streptomycin and 25 ug/mL gentamicin) and 400 µg/ml geneticin. Besides gentamicin (American Pharmaceutical Partners, IL) all antibiotics were purchased from Gibco/Invitrogen.

Human Umbilical Vein Smooth Muscle Cells

Human umbilical vein smooth muscle cells (HUVSMCs), purchased from the American Type Culture Collection (CRL-2481; ATCC, VA), were grown at 37°C with 5% CO₂ on 0.5% gelatin (porcine skin gelatin, Sigma-Aldrich, MO) coated dishes (Techno Plastic Products, Switzerland) in DMEM with Ham's F12 (Gibco/Invitrogen) in

ratio 3:1, 10% FBS, antibiotics (100U/mL penicillin streptomycin and 25 ug/mL gentamicin), 20 ug/mL Endothelial Cell Growth Supplement (ECGS, Upstate, CA), Sodium Pyruvate (NaPy, Gibco/Invitrogen) 0,1M.

Porcine Aortic Smooth Muscle Cells

Freshly isolated porcine aortic smooth muscle cells (PASMCS), kindly donated by Dr. Laura Niklason (Yale University, CT), were grown at 37°C with 5% CO₂ on 0.5% gelatin coated dishes in low glucose DMEM (Gibco/Invitrogen) with 10% Hyclone fetal bovine serum (Hyclone Laboratories, UT), 10% porcine serum (Invitrogen, CA), L-ascorbic acid, copper sulfate, HEPES, L-proline, L-alanine, L-glycine, and Penicillin G (all aforementioned supplements were from Sigma-Aldrich).

Human Umbilical Vein Endothelial Cells

Human umbilical vein endothelial cells (HUVECs), purchased from ATCC (CRL-1730) were grown at 37°C with 5% CO₂ on 0.5% gelatin coated dishes in F12K medium (Gibco/Invitrogen) supplemented with 10% FBS, 0.1 mg/ml heparin (Sigma-Aldrich), 20 µg/ml ECGS, 2 mM L-glutamine (Gibco/Invitrogen), antibiotics (100U/mL penicillin streptomycin).

Human Skin Fibroblasts

Human skin fibroblasts (HSFs), purchased from ATCC (CRL-2522), were grown at 37°C with 5% CO₂ on 0.5% gelatin coated dishes in DMEM with Ham's F12 in ratio 3:1, 20% FBS, antibiotics (100U/mL penicillin/streptomycin and 25 ug/mL gentamicin), glutamine 2mM, NaPy 0,1M.

Cryopreservation

All cells were cryopreserved at early passages and were stored in liquid nitrogen until needed for experimental procedures. Following trypsinization, cells were pelleted via centrifugation and resuspended in a freezing medium containing 10% dimethyl sulfoxide (DMSO, Acros organics, NJ) and 90% FBS. Cells were transferred to cryogenic screw cap vials (Fischer Scientific, PA) and frozen in freezing canisters (Nalgene, NY) containing room temperature isopropyl alcohol and incubated in a -80°C freezer for 24 hours. After 24 hours, vials were transferred to a liquid nitrogen tank for long term storage.

Microtissue fabrication

Multicellular spheroids preparation

Cell culture Petri dishes were washed twice with phosphate buffered saline solution (PBS, Gibco/Invitrogen) and treated for 10 min with trypsin (Gibco/Invitrogen) 0.1%. Cell solutions were subsequently centrifuged at 1,500 RPM for 5 min. In the case of HUVSMCs, HUVECs, HSFs, and PASMCS, cells were resuspended in 4 ml of cell-type specific medium and incubated in 10-ml tissue culture flasks (Bellco Glass, NJ) at 37°C with 5% CO₂ on gyratory shaker (New Brunswick Scientific, NJ) for about one hour, for adhesion recovery (usually marked by the formation of cell clusters). Cells were then resuspended and centrifuged again at 3,500 RPM. For all cell types, the resulting pellet was transferred into capillary micropipettes of 500 μm (Drummond Scientific Company, PA) or 300 μm (Sutter Instrument, CA) diameter and incubated at 37°C with 5% CO₂ for 15 min. The firm cylinders of cells removed from the pipettes were cut into 500-μm or 300 μm -long fragments (aspect ratio 1), then incubated in 10 ml tissue culture flasks with 3 ml of DMEM on a gyratory shaker at 120 RPM with 5% CO₂ at 37°C for 24–36 hours. Alternatively, microtissue fragments were incubated on agarose (Invitrogen) coated 96 well plates (Becton Dickinson Labware, NJ; one microtissue fragment per well) for 48 hours. This protocol reproducibly resulted in three-dimensional multicellular spheroids of similar size.

Cushion Tissue Spheroids Preparation

Leghorn chicken eggs (Ozark Hatcheries, MO) were incubated at 40°C in 80% humidity for 4–6 days. Excised cushion tissue explants were washed in Earle's Balanced Salt Solution (EBSS, Gibco/Invitrogen) and cut into similar size fragments. Fragments were incubated in a gyratory shaker (at 120 RPM with 5% CO₂ at 37°C) in DMEM supplemented with 10% FBS and 1% penicillin-streptomycin. In 24–36 hr (depending on initial fragment size), this procedure reproducibly yielded round tissue spheroids.

Multicellular cylinder preparation

Cell culture Petri dishes were washed twice with PBS, and then treated for 10 min with trypsin 0.1%. Cell solutions were subsequently centrifuged at 1,500 RPM for 5 min. In the case of HUVSMCs, HUVECs, HSFs, and PASMCS, cells were resuspended in 4 ml of cell-type specific medium and incubated in 10-ml tissue culture at 37°C with 5% CO₂ on gyratory shaker for about one hour, for adhesion recovery (marked by the formation of cell clusters); then cells were resuspended and centrifuged again at 2,500 RPM. For all cell types, the resulting pellet was transferred into capillary micropipettes of 500 µm or 300 µm diameter and incubated at 37°C with 5% CO₂ for 15 min. The firm cylinders of cells were extruded in adhesive-free grooves either manually or using the bioprinter (see Fig. 2) and incubated overnight at 37°C with 5% CO₂. This protocol reproducibly resulted in firm multicellular cylinders of similar size.

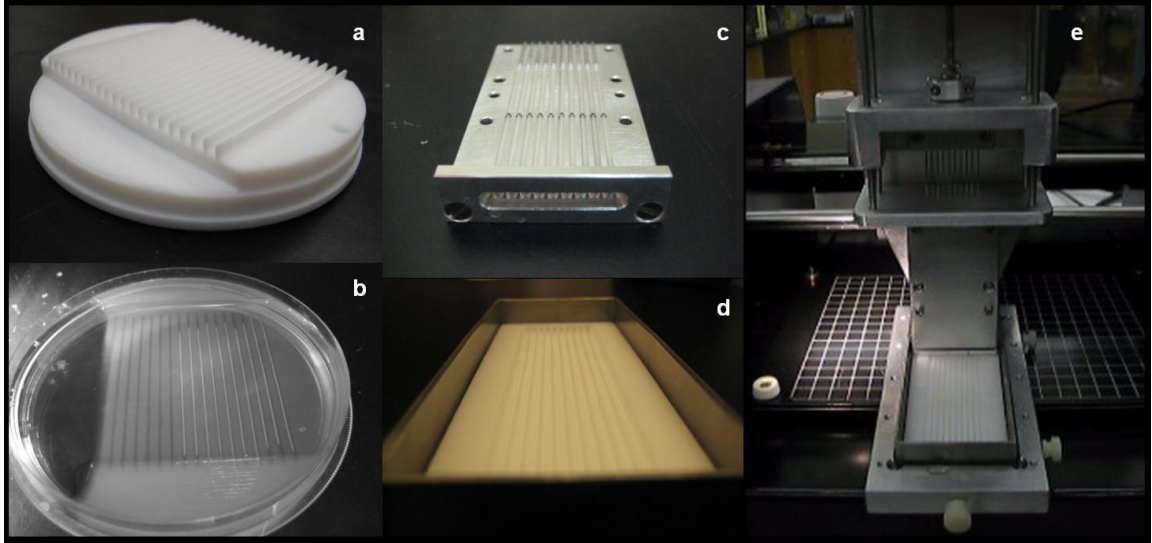


Figure 2. Multicellular cylinder Preparation. Multicellular cylinders were incubated in adhesive-free grooves made of agarose or Teflon. Agarose grooves were prepared by pouring liquid agarose into a negative Teflon mold (a) mounted on a Petri dish; after agarose gelation, the mold was removed, leaving behind straight agarose grooves in which multicellular cylinders were manually deposited (b). Computer-aided deposition was achieved by placing 10 micropipettes into a special cassette (c), then extruding the multicellular cylinders from the micropipettes simultaneously into Teflon grooves (d) using a specifically designed module mounted on the bioprinter (e).

Measurement of liquid interfacial tension and apparent tissue surface tension

The apparatus shown in Fig. 3 is designed to measure the equilibrium force resulting from the compression of one to several liquid droplets or tissue spheroids between two parallel plates. In order to determine the interfacial tension between two liquids, the inner chamber containing the plates was first filled with the liquid of lower volumic mass (olive oil or turpentine) before deposition of one or several liquid droplets (sizes ranged

from 250 μm to 500 μm in radii) of higher volumic mass (water) on the lower compression plate (LCP). For tissue droplets (175 μm to 300 μm in radii) compression, the inner chamber was filled with CO₂ independent medium (Gibco/Invitrogen). To assure constant temperature, a circulating water bath (Lauda, Germany) maintained the temperature of water in the outer chamber at 37°C. The upper compression plate (UCP) was then suspended from the arm of a electrobalance (Cahn/Ventron, CA) and the recording of its apparent weight was used to establish a precompression zero force baseline. Raising the lower plate compressed the liquid or tissue droplets between the two plates, the degree of compression being varied through adjustment of the height of the LCP. Changes in the force exerted by the drop upon the UCP, equal to the changes in the latter's apparent weight, were monitored by Labview software (National Instruments, TX). The shape of the droplets before, during and after compression, was recorded by a Spot Insight CCD camera (Diagnostic Instruments, MI) fitted to a horizontally positioned dissecting microscope (Olympus, Japan). Tissue apparent surface tension and liquids interfacial tension were determined from the compression force at equilibrium and from the shape of uncompressed and compressed tissue spheroids or liquid droplets according to the theoretical solution of Laplace equation developed in Chapter IV.

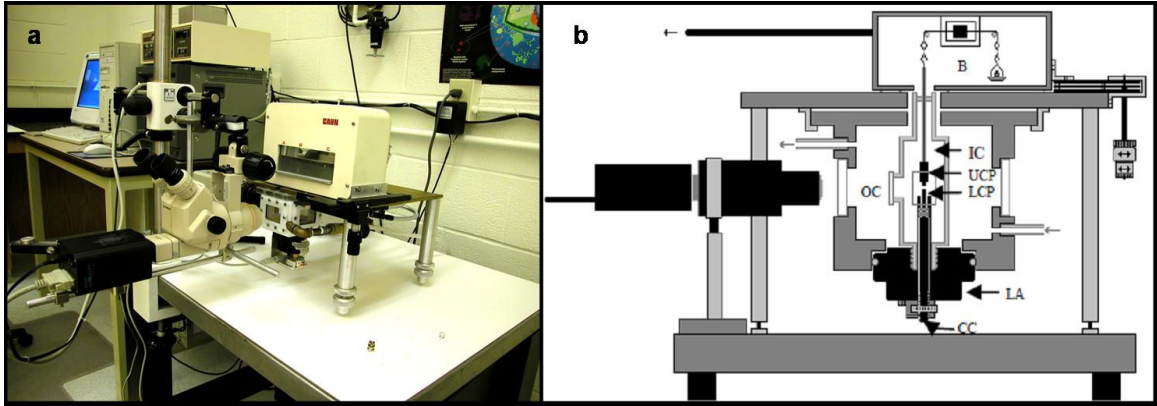


Figure 3. Parallel plate compression device for surface tensiometry. General view (a) and schematic view (b). The outer chamber (OC) is connected to a thermostatted circulating water pump and serves to regulate the temperature of the inner chamber (IC). The lower assembly (LA) screws into the base of the inner chamber. The position of its central core (CC), whose tip is the lower compression plate (LCP), can be adjusted vertically by a screw thread to set the distance between the two plates. The upper compression plate (UCP) is a cylinder about 12 mm long suspended from the arm of a recording electrobalance (B). Its position can be adjusted horizontally to place the UCP directly above the LCP. During an experiment, liquid droplets or tissue spheroids are positioned on the lower plate and raised until it contacts the upper plate. Compression of the droplets reduces the load measured by the balance by an amount equal to the force acting upon the droplets. Adapted from [44].

Segregation assays

Cell-sorting assay

The sorting pattern of mixed vascular cell types was assessed in binary combinations within a unique multicellular spheroid. Briefly, 300µm spheroids were prepared from mixtures of HUVECs with HUVSMCs, HUVSMCs with HSFs, and HSFs with HUVECs, previously stained with green and red intercalating fluorescent membrane dyes (SP-DiI_{C18} and SP-DiOC₁₈; Molecular Probes, OR). They were then incubated at 37°C with 5% CO₂ for 24 to 36 hours on gyratory shaker (120 RPM) or static (i.e agarose bed) conditions. Cell-sorting was evaluated every 2 hours at 60 µm depth using a LSM510 Meta confocal microscope (Zeiss, NY).

Tissue-envelopment assay

The ability of vascular cell types to spread upon each other was assessed in binary combinations of single-cell type multicellular spheroids brought in contact with one another. Single-cell type 300 µm spheroids were prepared from HUVECs, HUSMCs and HSFs previously stained with green and red intercalating fluorescent membrane dyes. Two spheroids were placed side-by-side in binary combinations of distinct vascular cell types (for example one HUVEC spheroids in contact with one HSF spheroid) on agarose bed (in 96-well plates). Spreading of one spheroid over the other was evaluated using a MZFLIII fluorescence stereomicroscope (Leica, IL) every 2 hours.

Macrotissue fabrication

Microtissues (multicellular spheroids or cylinders) composed of various cell types (CHO, HUVSMCs, HSFs, HUVECs, PASMCS) were assembled layer by layer, concomitantly with 2% agarose cylinders, either manually or using bioprinting into custom-shaped tubular patterns. Here we describe the materials used; details on the method are given in Chapter V.

For sterility reasons, manual assembly was carried out in a biosafety level II cabinet using video-assistance: a 5000 Coolpix Camera (Nikon, Japan) mounted on a dissecting microscope and connected to a video monitor (Sharp, Japan) as shown in Fig. 4.

The bioprinter is a modified version of the Roland MDX-20 milling machine (Roland DGA, CA), originally developed to create molds for the plastics industry. It consists of an X-Y two dimensional stage and a Z assembly, housing a drill or knife. The cutting device was replaced by two vertically moving linear displacement extruders (Fishman, MA). Each extruder was fitted with a syringe holding a glass micropipette (Drummond Scientific) with a steel wire piston inserted. One fully assembled extruder with its piston, syringe and micropipette constitutes a “printing head”: one is devoted to agarose printing, the other to multicellular spheroid or cylinder printing.



Figure 4. Manual and computer-aided tissue assembly system. Manual macro-tissue assembly was performed in a biological safety cabinet using video assistance (**top left**). Computer-aided assembly was performed using a specifically designed bioprinter (**bottom left**): the stage supports a Petri dish in which the tissue construct is printed, and two temperature-controlled chambers in which cold or hot water is circulated (**top right**); the printing heads consist of an extruder fitted with a syringe holding a glass micropipette with an inserted piston (**bottom right**).

The control unit of the dispensers is connected to and operated by the printer. The printer itself is operated (X movements of the stage, Y-Z movements of the printing heads, dispenser control) by a computer through scripts in RML-1 programming language

(Roland). In order to evaluate the position of the printing micropipettes, and to record the printing process, a video camera (Panasonic, Japan) was attached directly to the stage. Two specifically designed constant-temperature chambers were mounted on the stage, to house warm liquid agarose and cold PBS. Hot water was circulated with a peristaltic mini-pump (Fisher Scientific, NH) through the liquid agarose-containing chamber using a temperature-controlled water bath. In the same manner, cold water was circulated through the PBS containing chamber.

Maturation of engineered vascular constructs

Engineered vascular constructs made from PSMCs were matured for a maximum of 6 weeks under pulsatile flow. For this purpose, constructs were first mounted in specifically designed perfusion bioreactor made of polycarbonate (Fig. 5). Vascular constructs were attached to specific-size needles (Hamilton, NV; Small Parts Inc.) using microvascular clamps (S&T, Switzerland) or 7-0 Silk Black braided surgical thread (Ethicon, GA). Needles were secured using silicone stoppers (Cole-Parmer, IL), that further prevented any leakage from the bioreactor. Masterflex tubing (Cole-Parmer) was used for all connections in conjunction with polypropylene connectors (Cole-Parmer). Throughout the maturation, 5% cyclic strain was applied to the vascular constructs by adjusting the speed of a peristaltic pump (Cole-Parmer). Engineered constructs were cultured in PSMC-specific medium. Gas exchange and medium renewal (every three days) was assured through the 0.2 μm PTFE filters (Cole-Parmer) and the injection ports (Baxter, Singapore) of the bioreactor and the medium reservoir.

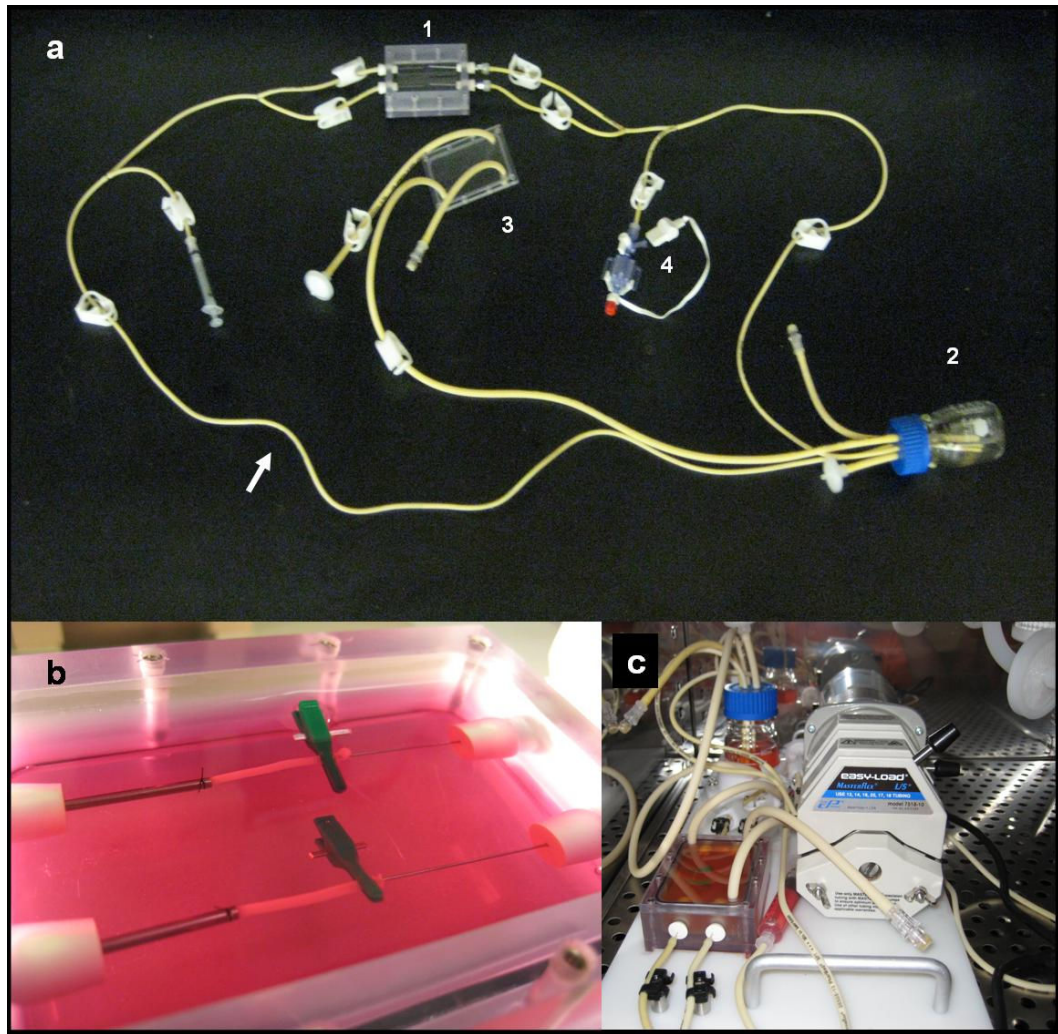


Figure 5. Perfusion Bioreactor. Perfusion system for vascular construct maturation was assembled as shown in (a). The bioreactor (a1) allows for the simultaneous perfusion of two engineered vascular constructs (b). A peristaltic pump inserted in the circuit (a, arrow) creates a pulsatile flow responsible for the cyclic radial strain of the constructs. Pressure is measured through a pressure transducer (a4) in order to monitor any leakage in the circuit. Bioreactor lid (a3) allows for gas exchange (filter) and medium renewal (injection port) as well as medium reservoir (a2). Once assembled, the perfusion system is placed in the incubator (c) at 37°C with 5% CO₂ for a maximum of 6 weeks.

Microscopy

Histological and immunohistochemical analysis

Tissues were fixed overnight in 4% paraformaldehyde (Electron Microscopy Sciences, PA) for routine microscopy and immunohistochemistry. Dehydration was performed by an increasing concentration series of ethanol as follows: 10%, 25%, 50%, and 70% for 30 min each. Tissues were routinely processed for paraffin infiltration and embedding. Sections (5 μ m) were mounted onto ProbeOn Plus microscope slides (Fisher Scientific) and some were stained with hematoxylin-eosin for global aspect and cellularity, picrosirius red for fibrillar collagen, Verhoeff van Gieson's for elastin.

Before immunohistochemistry, sections were dewaxed in xylene, rehydrated through graded concentrations of ethanol, then rinsed in distilled water, and, if necessary, stored in PBS at 4°C until use. Sections were subjected to heat-induced epitope retrieval method for 20 minutes in either 1 mM/L TRIS buffer, 1mM EDTA (pH 9.0; Dako Target Retrieval Solution, High pH, code No. S 3308, CA) for CD31 immunohistochemistry, or 10mM/L citrate buffer (pH 6.0; Dako Target Retrieval Solution, Low pH, code No: K8015) for cleaved caspase-3 and smooth muscle actin assays. Slides were treated with 3% H₂O₂ in absolute methanol (to inactivate endogenous peroxidase activity) before being washed in 3x PBS and then immersed in 10% bovine serum albumin for 20 minutes. Sections were incubated for 60 minutes at room temperature with each of the following antibodies: anti-CD31 antibody [1:40 dilution of a mouse anti-human CD31 monoclonal antibody (JC70A) that reacts with the 130kD CD31 molecule); Dako]; anti-cleaved

caspase-3 (1:50 dilution of a rabbit anti-cleaved caspase-3 polyclonal antibody that reacts with mouse and human cleaved caspase-3, Trevigen, MD); PCNA [1:500 dilution of mouse anti-rat monoclonal antibody (M0879); Dako]; and anti-smooth muscle actin [1:400 dilution of a mouse anti-human smooth muscle actin (1A4), Dako]. Sections were then washed and sequentially incubated with a secondary antibody (EnVision+, a horseradish peroxidase-labeled polymer conjugated with either anti-mouse or anti-rabbit antibodies; Dako) for 30 minutes at room temperature. Bound antibodies were visualized following incubation with a substrate for bound horseradish peroxidase using either NovaRED substrate for CD31 (Vector Laboratories, CA) or DAB (3, 3'-diaminobenzidine tetrahydrochloride) 0.05% with 0.015% H₂O₂ in PBS for 3 to 5 minutes. Sections were counterstained with Mayer's hematoxylin, dehydrated, cleared, and coverslipped for microscopic examination (IX70; Olympus, NY).

Cell Viability and Proliferation

Cell viability and proliferation assessment in tissue-engineered constructs was performed using respectively Caspase-3 (apoptotic cells) and PCNA (proliferating cell nuclear antigen) immunostainings as described above.

Visualization of cell-segregation patterns

To visualize the details of fusion, sorting, and spreading of multicellular spheroids composed of CHO cells, HUVSMCs, HUVECs, or HSFs, these were stained with red and

green membrane-intercalating dyes (SP-DiI_{C18} and SP-DiOC₁₈; Molecular Probes, OR) according to the protocol supplied by the manufacturer, prior to multicellular spheroid preparation.

Scanning Electron Microscopy of multicellular spheroids surface

The morphology of cells on the surface of multicellular spheroids was analyzed by FESEM (Field Emission Scanning Electron Microscopy). Spheroids were fixed in 4% paraformaldehyde (Electron Microscopy Sciences) in PBS for 90 min, on a low speed shaker. Subsequently, samples were rinsed 3 times for 10 min in PBS. Dehydration was performed by an increasing concentration series of ethanol as follows: 10%, 25%, 50%, 75%, 95%, for 30 min each and finally in 100% ethanol overnight. After critical point drying (Samdri-PVT-3B, Tousimis, MD), aggregates were spread on carbon adhesive tabs mounted on stub and sputter coated with platinum to a nominal thickness of 2 nm. Aggregate surface was examined using a S4700 cold-cathode field-emission scanning electron microscope (Hitachi, Japan) at an accelerating voltage of 5 kV.

CHAPTER IV: “LIQUID-LIKE” PHENOMENA GOVERN SELF-ASSEMBLY OF VASCULAR CELLS INTO MICROTISSUE *IN VITRO*

Introduction

In this chapter, we evaluate the liquid-like properties of reconstituted microtissues composed of the three main vascular cell types (i.e., endothelial cells, smooth muscle cells and fibroblasts). Although microtissues made from aggregated cells commonly display elastic behavior on short time scale (i.e, a few seconds to several minutes), they behave like viscous fluids on the long time scale (i.e., a few hours) [91]. *In vitro* phenomena relating to this similarity include rounding-up into multicellular spheroids, fusion of spheroids, or even cell segregation (illustrated by cell-sorting or tissue envelopment events). In the latter case, equilibrium configurations resulting from the segregation of two distinct cell types can be predicted on the basis of tissue surface tension, measured by a surface tensiometer (i.e. parallel plate compression apparatus, Fig. 3) [59, 91]. Tissue surface tension (denoted by σ) reflects intercellular cohesion mediated by adhesion molecules [64]. It guides *in vitro* self-assembly of multicellular microtissues into segregated domains, the more cohesive tissue (of higher surface tension) being surrounded by the less cohesive one (of lower surface tension) [60]. (We also verified that spheroid surface tension was independent of spheroid size, compression force, and degree of compression exerted upon it.) Surface tension is evaluated from compression measurements and is based on the Laplace equation. Earlier approaches that used

simplifying assumptions on the solution of the Laplace equation, often led to spurious results. To avoid inconsistencies we exactly solved the Laplace equation for the profile of the compressed aggregate. We tested the method by determining the interfacial tensions between true liquids (water, turpentine, olive oil). The exact solution provided the theoretical basis to evaluate the liquid-like properties of various tissues including smooth muscle cell-, endothelial cell-, and fibroblast spheroids using tissue surface tensiometry. The exact solution provided further support to the notion of tissue surface tension, as it was found independent of spheroid size, compression force, and degree of compression. Finally we investigated the role of tissue surface tension in guiding the self-assembly of distinct vascular cell types, by conducting *in vitro* cell-sorting and tissue-envelopment assays.

Surface tension: theoretical considerations

Formulation of the mathematical problem for the relevant experimental conditions

For a small liquid droplet compressed between two parallel plates, the surface tension σ can be determined from its geometric shape (Fig. 6). We consider droplets with radius R_0 smaller than the millimetric capillary length $R_c \approx (\sigma/\rho g)^{1/2}$, for which the effect of gravity can be neglected. (For water $R_c \approx 2.6$ mm, while for cellular aggregates considered here $R_c > 1$ mm.) The shape of such a liquid drop placed on a horizontal plate (Fig. 6A) is a spherical cap of radius R_{10} and height H_0 . In terms of these parameters, the

(external) contact angle $\theta = \cos^{-1}(H_0/R_{10} - 1)$ and, assuming incompressibility, the radius of the suspended drop, $R_0 = R_{10} \left[(2 - \cos\theta) \cos^4(\theta/2) \right]^{1/3}$. While H_0 and R_{10} can be measured with high accuracy (e.g., ~1%), the relative error $\Delta\theta/\theta \approx \left[(1 + \cos\theta)/\theta \sin\theta \right] (\Delta H_0/H_0 + \Delta R_{10}/R_{10})$ can still be very large (e.g., ~130% for $\theta < 10^\circ$). Thus, to accurately determine θ , it is desirable to avoid using quantities that explicitly contain the contact angle.

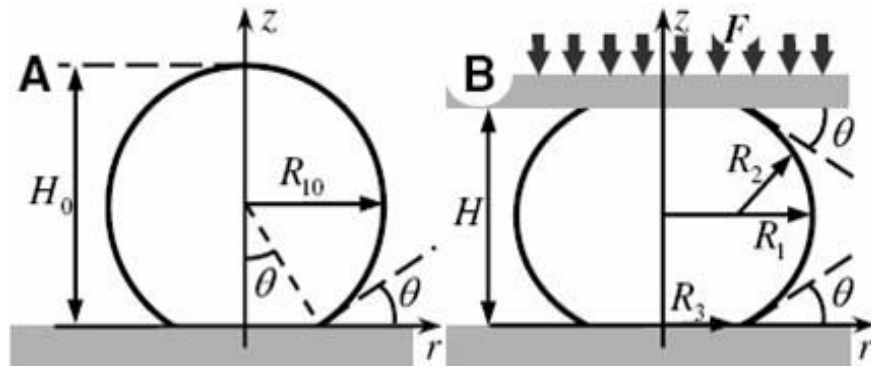


Figure 6. Schematic diagram of (A) an uncompressed and (B) a compressed liquid drop, at shape equilibrium.

The compressed drop has rotational symmetry about the z -axis and reflection symmetry with respect to its equatorial plane, in which it has the two principal radii of curvatures R_1 and R_2 shown in Fig. 6B. R_3 is the radius of the droplet's circular area of contact with the compression plates. The magnitude of compression depends on the compression force F applied to the upper (or lower) plate. In terms of R_1 and R_2 , the excess pressure inside the drop due to the surface tension is given by the Laplace formula $\Delta p = \sigma(1/R_1 + 1/R_2)$.

In the compressed state of the drop, the mechanical equilibrium condition, when evaluated at the upper plate, leads to

$$F = \pi\sigma \left[R_3^2 \left(1/R_1 + 1/R_2 \right) - 2R_3 \sin \theta \right] \quad (1a)$$

Here we employed the Laplace equation to eliminate Δp .

Similarly, in the equatorial plane, we have

$$F = \pi\sigma R_1 \left(R_1/R_2 - 1 \right). \quad (1b)$$

In addition to H , R_1 and F (which can be accurately measured), to determine σ directly from either of these two equations, requires the quantities R_2 , θ and R_3 that can only be measured with large errors. In earlier studies this problem has been circumvented by assuming $\theta = 0$ (no adhesion to the plates) and/or making approximations on the lateral profile of the drop, e.g., $R_3 = R_1 - R_2$ (the profile is a semicircle) or $R_3 = R_1 - R_2 + \left[R_2^2 - (H/2)^2 \right]^{1/2}$ (the profile is a circular arc) [60, 91]. Each of these schemes fails to give consistent results in some range of the compressive force or contact angle. For example, approximating the lateral profile with a circular arc implies that the contact angle depends on the magnitude of the compressive force, an unphysical conclusion.

Exact solution of the Laplace equation: the surface tension in terms of experimentally measurable quantities

Determining R_1 , R_2 and R_3 requires the exact profile $z(r)$ of the compressed liquid droplet, which can be obtained by the exact integration of the Laplace equation

$$\Delta p = \sigma \left[\frac{z'}{r(1+z'^2)^{1/2}} + \frac{z''}{(1+z'^2)^{3/2}} \right] = \text{const} , \quad (2)$$

subject to the boundary conditions (see Fig. 1B)

$$\begin{aligned} z(R_3) &= 0, & z'(R_3) &= \tan \theta, \\ z(R_1) &= H/2, & z'(R_1) &= \infty. \end{aligned} \quad (3)$$

The terms in the square brackets in eq. (2) represent the principal curvatures of the drop's surface at a point determined by $z(r)$. In the above equations z' and z'' represent the first and second derivatives of the function $z(r)$.

We are now in the position to determine σ in terms of the easily and accurately measurable quantities H , R_1 and F . Equations (1) imply that both R_2 and R_3 can be expressed in terms of R_1

$$R_2 = R_1/(2\alpha - 1), \quad R_3 = \beta_\theta R_1, \quad (4a)$$

where the dimensionless parameters α and β_θ are given by

$$\alpha = \Delta p / (2\sigma / R_1), \quad (4b)$$

$$\beta_\theta \equiv \beta_\theta(\alpha) = \frac{\sin \theta + \sqrt{\sin^2 \theta + 4\alpha(\alpha - 1)}}{2\alpha}. \quad (4c)$$

Integrating eq. (2) with the boundary conditions (3) leads to an implicit equation for α

$$\begin{aligned} \frac{H}{2R_1} &= f_\theta(\alpha) \equiv \int_{\beta_\theta}^1 z'(x) dx, \\ z'(x) &= \left[\left(\frac{x}{\alpha x^2 + 1 - \alpha} \right)^2 - 1 \right]^{-1/2}, \end{aligned} \quad (5)$$

and the lateral profile of the compressed drop

$$z(r) = R_1 \int_{\beta_\theta}^{r/R_1} z'(x) dx. \quad (6)$$

The α -dependence of the functions $f_\theta(\alpha)$ and $\beta_\theta(\alpha)$ is shown in Fig. 7 for several values of the contact angle (i.e., $\theta = 0^\circ, 10^\circ, \dots, 40^\circ$). By simple inspection one can see that $\beta_\theta(\alpha)$ has a much stronger θ -dependence than $f_\theta(\alpha)$. In fact, one finds that $f_\theta(\alpha) \approx f_0(\alpha)$ is an excellent approximation for $\theta \leq 20^\circ$. Thus, for small contact angles, it follows that $\alpha = f_0^{-1}(H/2R_1)$ and, therefore, R_2 are relatively insensitive to even large (e.g., $\sim 10^\circ$) sample-to-sample fluctuations of θ (e.g., caused by local inhomogeneities or impurities). By contrast, since β_θ itself strongly depends on θ , so does R_3 . This explains why its determination by fitting the lateral profile of the drop by circular arcs leads to sizable errors.

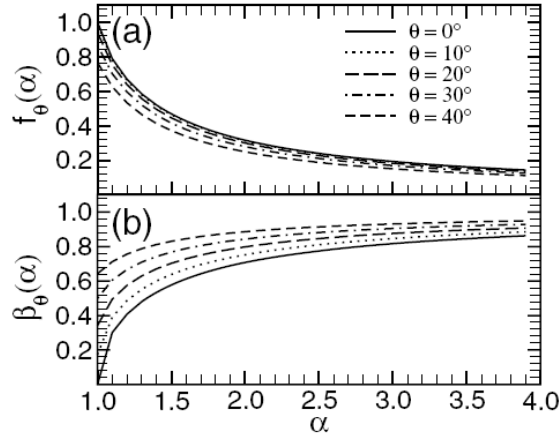


Figure 7. Plot of (a) $f_\theta(\alpha)$, and (b) $\beta_\theta(\alpha)$ for different values of the contact angle θ .

Finally, σ can be expressed from either eq. (1a) or (1b), which in terms of $\alpha = f_\theta^{-1}(H/2R_1)$ (see eq. (5) and Fig. 6a) can be rewritten as

$$F/2\pi R_1 = \sigma(\alpha - 1). \quad (7)$$

For sufficiently weak adhesion between the liquid drop and compression plates (i.e., $\theta \leq 20^\circ$), this result provides a simple recipe to evaluate σ from the measurement of only H , R_1 and F . Namely, σ is given by the slope of the least square linear fit to the experimentally measured data points $\{f_\theta^{-1}(H/2R_1) - 1, F/2\pi R_1\}$, that goes through the origin.

Generalization to simultaneous compression of several droplets

The efficiency of the proposed method for measuring σ can be further enhanced by simultaneously compressing several ($n=1, \dots, N$) drops, as shown in Fig. 8B. For such compressions the quantities $F/2\pi R_1$ and α in eq. (7) need to be replaced, respectively by $F/2\pi \bar{R}_1$ and $\bar{R}_1^{-1} \sum_n R_{1n} \alpha_n$, with $\bar{R}_1 = \sum_n R_{1n}$ and $\alpha_n = f_\theta^{-1}(H/2R_{1n})$.

Incompressibility

It should be emphasized that eq. (5) is valid for incompressible and compressible liquids alike. For incompressible liquids, volume conservation yields:

$$(R_0/R_1)^3 = g_\theta(\alpha) \equiv (3/2) \int_{\beta_\theta}^1 x^2 z'(x) dx. \quad (8)$$

Similarly to the function $f_\theta(\alpha)$, for $\theta \leq 20^\circ$, one finds that to a very good approximation

$g_\theta(\alpha) \approx g_0(\alpha)$. Eliminating α between eqs. (5) and (8) leads to

$$(H/2R_1) = U_\theta(H/2R_0) \approx U_0(H/2R_0), \quad (9)$$

where U_0 is a universal function defined through: $U_0(x) = f_0(\alpha)$ and

$x = f_0(\alpha)[g_0(\alpha)]^{1/3}$. Thus, for weak adhesion between the drop and plates (i.e., $\theta \leq 20^\circ$)

there is a universal relationship between $H/2R_1$ and $H/2R_0$, valid for any

incompressible liquid drop regardless of its type or size.

Interfacial and surface tension measurement of liquids, tissues, and multicellular spheroids

We have tested the above theory to determine the interfacial tension of true immiscible liquids (water in olive oil (W-O) and turpentine (W-T)), where results obtained by other methods are available. Subsequently, we applied the analytical results to obtain the absolute values of tissue surface tensions. Measurements were performed using a specifically designed compression tensiometer (See Materials and Methods). In the case of ordinary liquids compressions were performed on one or simultaneously two spherical water drops of various size (ranging from 0.4 to 1mm in diameter) (Fig. 8B). In each experiment, drops were exposed to at least 3 successive compressions (up to 9) of increasing force and their profile was recorded at shape equilibrium.

For biological measurements we either used intact tissue (fragments of excised embryonic chicken cardiac cushions (CT) that round into spheres in about 12 hours) or multicellular spheroids composed of various cell types, including vascular such as smooth muscle cells (HUVSMCs), endothelial cells (HUVECs) and fibroblasts (HSFs). Spheroids were prepared as previously described [10] (and see Materials and Methods). They were then compressed in culture medium at 37°C (Fig. 8A). One to six spheroids of each type were compressed simultaneously. In order to avoid irreversible damage to the cells, no more than two compressions were performed on any spheroid.

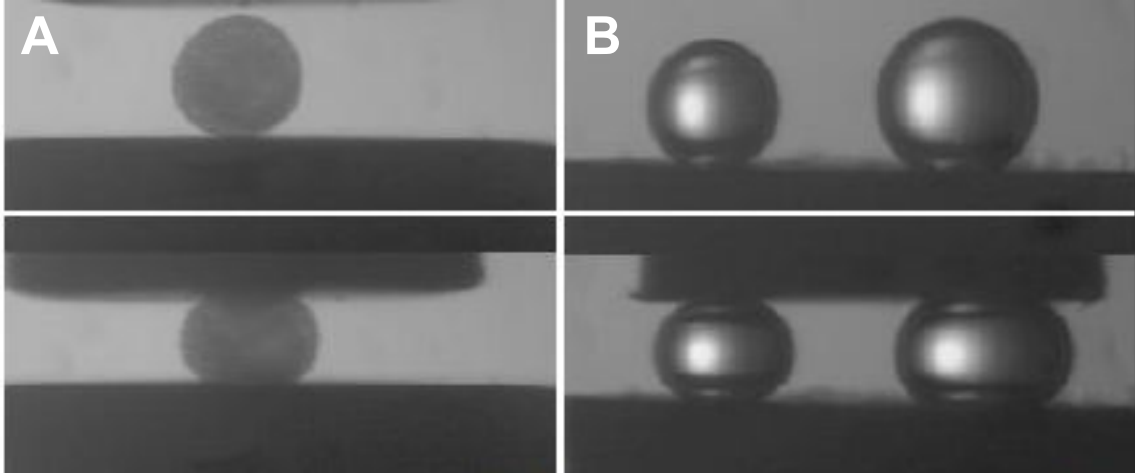


Figure 8. Compression of liquid droplets and tissue spheroids. (A) Snapshots of uncompressed (top) and compressed (bottom) cushion tissue spheroids in culture medium. (B) Same for water drops in olive oil (W-O). The diameter of the uncompressed CT and the smaller W-O drops were 0.402mm and 0.441mm, respectively.

Upon compression cellular aggregates relax to equilibrium in a manner typical for viscoelastic materials [91]. As demonstrated earlier, by the end of this relaxation process the initially compressed cells regain their pre-compressed shape [117]. Since compression leads to the increase of the surface area, this implies that cells from the interior of the aggregate have to migrate to the surface (provided volume remains constant).

According to equation (7), for liquids, the pairs of data points $\{\alpha - 1, F / (2\pi R_1)\}$ should lie on a straight line passing through the origin, with σ given by the slope of the line. The data are shown in Fig. 9 and the obtained results are summarized in Table 1. In addition to the values of σ , the table also contains the standard deviation ($\Delta\sigma$), the corresponding percentage relative errors ($\Delta\sigma/\sigma$) and the total number of data points used in Fig. 9.

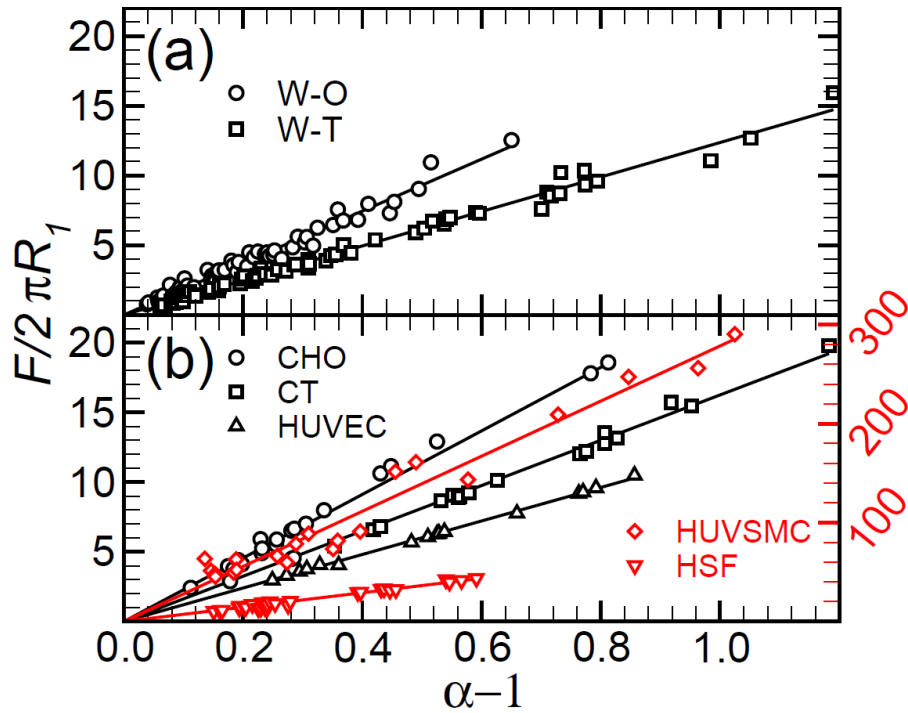


Figure 9. Employing eq. (7) for data evaluation. The surface or interfacial tensions are obtained from the slopes of the linear fit to the data points including the origin: (a) pure liquid (W-O, W-T), and (b) tissue and multicellular spheroids (CT, CHO, HUVEC, HUSMC, HSF). As indicated by the red color, the vertical axis on the right corresponds to HUSMC and HSF.

Results for W-O ($18.6 \pm 2.4 \text{ mN/m}$) and W-T ($12.4 \pm 1.5 \text{ mN/m}$) compare well with published data [12] (17 mN/m and 13.7 mN/m , respectively). The corresponding relatively large errors ($\sim 12\%$) in Table 1 reflect the sample sensitivity of σ and not a deficiency of the method. Indeed, the large number of W-O and W-T compression measurements (see table 1) were done in the course of four days, each time using different samples and compression plates. Most of these experiments were carried out on single droplets, which might have experienced somewhat different environmental conditions (sample-to-sample fluctuations). The actual errors $\Delta\sigma$ corresponding to drops from the same batch were

much smaller ($\sim 1\%$). Another possible source of error is related to the extent of compressions. Weaker compressions result in larger errors. From eq. (7), $\Delta\sigma/\sigma = \Delta F/F + \Delta R_1/R_1 + \Delta\alpha/(\alpha - 1)$ which may become large when $F \rightarrow 0$ and $\alpha \rightarrow 1$.

System	σ (mN/m)	$\Delta\sigma$ (mN/m)	$\Delta\sigma/\sigma$ (%)	Data points
W-O	18.6	2.4	12.9	56
W-T	12.4	1.5	12.1	60
CT	16.3	0.2	1.2	17
CHO	22.8	3.0	13.2	22
HUVEC	12.0	0.2	1.7	16
HUVSMC	279	57	20.4	21
HSF	72.7	7.5	10.3	30

Table 1. Interfacial and surface tensions of liquids, tissue and multicellular spheroids. Obtained from Fig. 9. The absolute errors $\Delta\sigma$ are standard deviations. The last two columns contain respectively the percentage relative errors $\Delta\sigma/\sigma$ and the number of data points.

For tissue fragments and cell aggregates σ s were determined by a similar procedure, with the results shown in Fig. 9b and Table 1, which clearly demonstrate that embryonic tissues and cell aggregates have well defined (apparent) surface tensions that are independent of their size or extent of compression. Measurements on CT and HUVEC were carried out with simultaneously prepared spheroids, which explains the small $\Delta\sigma$. These spheroids were exposed to multiple multi-aggregate compressions: five or six aggregates compressed twice. CHO aggregates also originated from a single batch, but compressions were performed on both single and multiple (two to five) aggregates, resulting in error similar to that of W-O and W-T. For HUVSMC four different batches of aggregates were used and, due to the large forces needed, only single aggregate

compressions were performed. This may explain the relatively large error ($\sim 20\%$). The above results on the values of the tensions suggest that multi-aggregate compression with aggregates from a single batch is the most accurate way of experimentally determining σ .

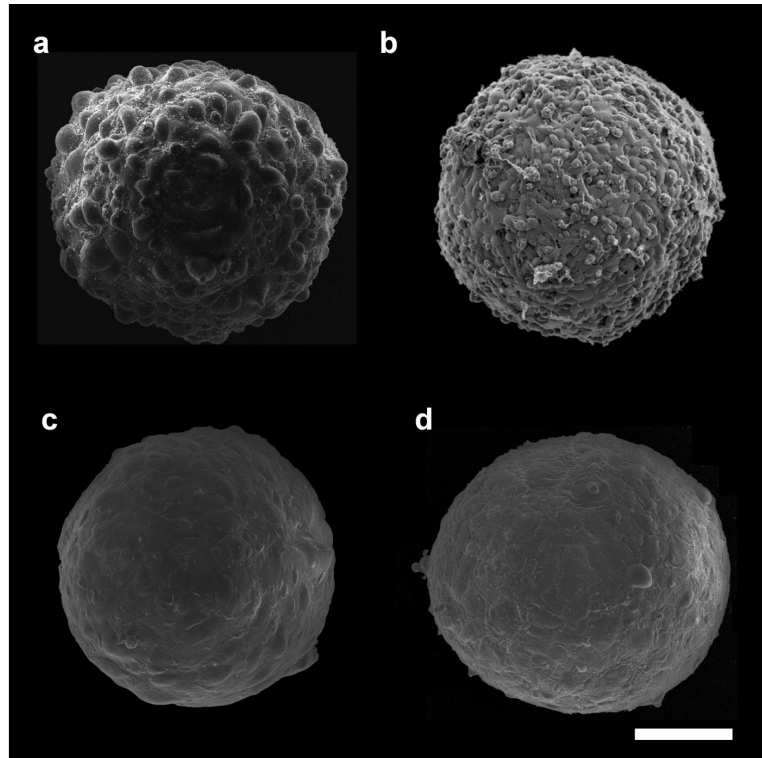


Figure 10. Scanning electron micrographs of multicellular spheroids. The berry-like appearance of HUVEC (**a**) and CHO (**b**) spheroids reveals limited adhesion between surface and subsurface cells. In contrast, the flattened shape of HSF (**c**) and HUVMSC (**d**) spheroids implies that surface cells adhere more strongly to subsurface cells and/or possibly illustrates cortical tension of surface cells (see text). Scale bar corresponds to 100 μm .

In light of the earlier discussed relationship between tissue surface tension and the intensity of binding between the constituent cells, our results suggest that smooth muscle cells adhere to each other with considerably greater strength than the other cell types

studied here. This suggestion is further supported by Fig. 10. The strong adhesion between smooth muscle cells may be consistent with their physiological role. These cells reside within the walls of hollow organs (e.g. bladder, vasculature) that are exposed to great mechanical load. Whereas it is well demonstrated that most of the arterial wall stress is supported by collagen fibers, it is also known that upon arterial wall injury, smooth muscle cells quickly migrate and proliferate at the lesion site [118]. Thus one can hypothesize that, because of their high cohesion (the strongest that has ever been measured on a tissue or cell type by tensiometry), they act as a first barrier (or “glue”) to preserve the physical integrity of the vascular wall. However, as we mentioned earlier, cell surface contraction may also contribute positively to surface tension. In the case of HUVMSCs which can exhibit a contractile phenotype illustrated by the expression of smooth-muscle α -actin for example, this could explain both their surprisingly high surface tension compared to other cell types, and the flat surface of HUVMSC spheroids (it was indeed shown in a recent study of gastrulation that flat spheroid surface could coincide with cortical expression of F-actin by surface cells [119]). Finally, the fact that the data points $\{H/2R_0, H/2R_1\}$ for all our measurements fall on the universal curve predicted by eq. (9) (Fig. 11) confirms that the multicellular systems studied here, similarly to water, are incompressible and provides an additional validation for our method.

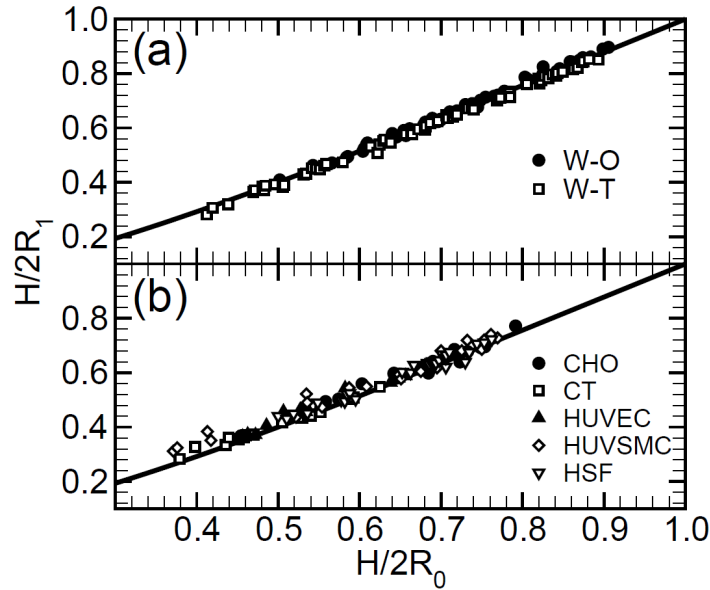


Figure 11. Testing incompressibility through the universal function given in eq. (9) (solid curve) to assess the incompressibility of the liquid drops (a) and the tissue and multicellular spheroids (b) used in the compression measurements.

Surface tension guides the self-assembly of vascular cells *in vitro*

By analogy with true immiscible liquids, the Differential Adhesion Hypothesis proposed that segregation phenomena of differentially adhesive cells should lead to an equilibrium configuration of minimal surface energy (equivalent to a maximal binding energy) where the most cohesive cells (of higher surface tension) are surrounded by the less cohesive cells (of lower surface tension). If energetically favored, this equilibrium configuration should eventually be reached from any initial starting configuration and reveal the operation of a strict rule of transitivity (Fig. 12).

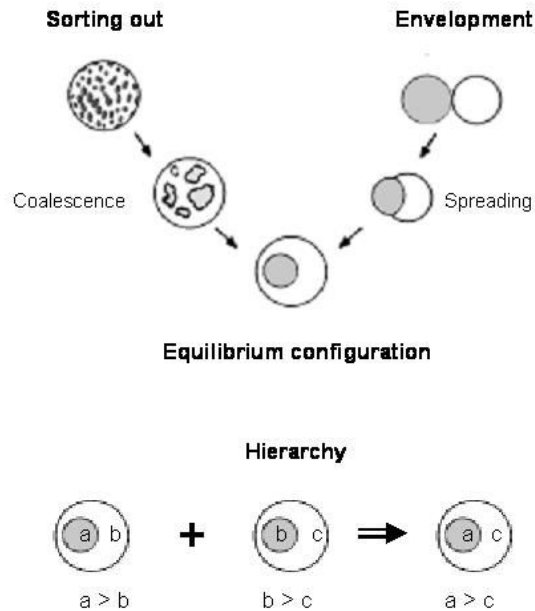


Figure 12. Liquid-like segregation of multicellular spheroids. (Top) Mixtures of differentially adhesive cells sort out by a process similar to coalescence of immiscible liquid droplets, forming a continuous external multicellular domain which envelops, to a greater or lesser degree, an internal domain. When brought together as separate masses, two spheroids composed of distinct cell populations spread, one upon the other, to approach the same (equilibrium) configuration reached by sorting-out. (Bottom) In a set of differentially adhesive cell populations, the tendencies of one population to spread over another are transitive; i.e., if b tends to spread over a and c tends to spread over b, then c will tend to spread over a. Adapted from [120].

We tested this prediction for the segregation behavior of the three main vascular cell types (i.e., smooth muscle cells, fibroblasts and endothelial cells) using two types of cell segregation assays previously developed *in vitro*: the cell-sorting assay and the envelopment assay (also called engulfment or spreading assay) summarized in Fig. 12. Briefly, the cell-sorting assay tests the ability of mutually but yet differentially adhesive

cell populations mixed together to sort out in distinct anatomical domains, while the envelopment assay tests the ability of apposed multicellular spheroids composed of distinct cell populations to spread upon one another.

According to the DAH, we predicted that, in the equilibrium state of the true binary combinations, HUVMSCs, the most cohesive cell type ($\sigma = 279$ dynes/cm), would be surrounded by the other two cell types, HUVECs ($\sigma = 12$ dynes/cm) and HSFs ($\sigma = 64$ dynes/cm). In turn, HUVECs, being the least cohesive cell type, would be surrounding the other two cell types (HUVMSCs or HSFs). Finally HSFs would surround HUVMSCs but be surrounded by HUVECs. As mentioned above, such equilibrium configurations would arise either through sorting or envelopment (Fig. 12). For envelopment assays, briefly, cells were labeled with green or red fluorescent membrane dyes; then similar size ($\sim 300 \mu\text{m}$) multicellular spheroids composed of one vascular cell type were prepared (see material and methods) and apposed in pairs on agarose bed: the binary combinations tested here were HUVEC-HUVMSC, HUVEC-HSF and HUVMSC-HSF. Spreading was followed for at least 72 hours under a fluorescence stereomicroscope until equilibrium configuration was reached. For sorting experiments, briefly, after trypsinization, fluorescently labeled cells were mixed according to the following proportions: HUVMSC-HUVEC (80%-20%), HUVMSC-HSF 50%-50%, HSF-HUVEC (80%-20%). Mixed spheroids ($\sim 300 \mu\text{m}$) were prepared as explained in 3.2.1 and incubated either in static conditions (agarose bed) or on gyratory shaker. Sorting was followed for at least 24 hours with a confocal microscope.

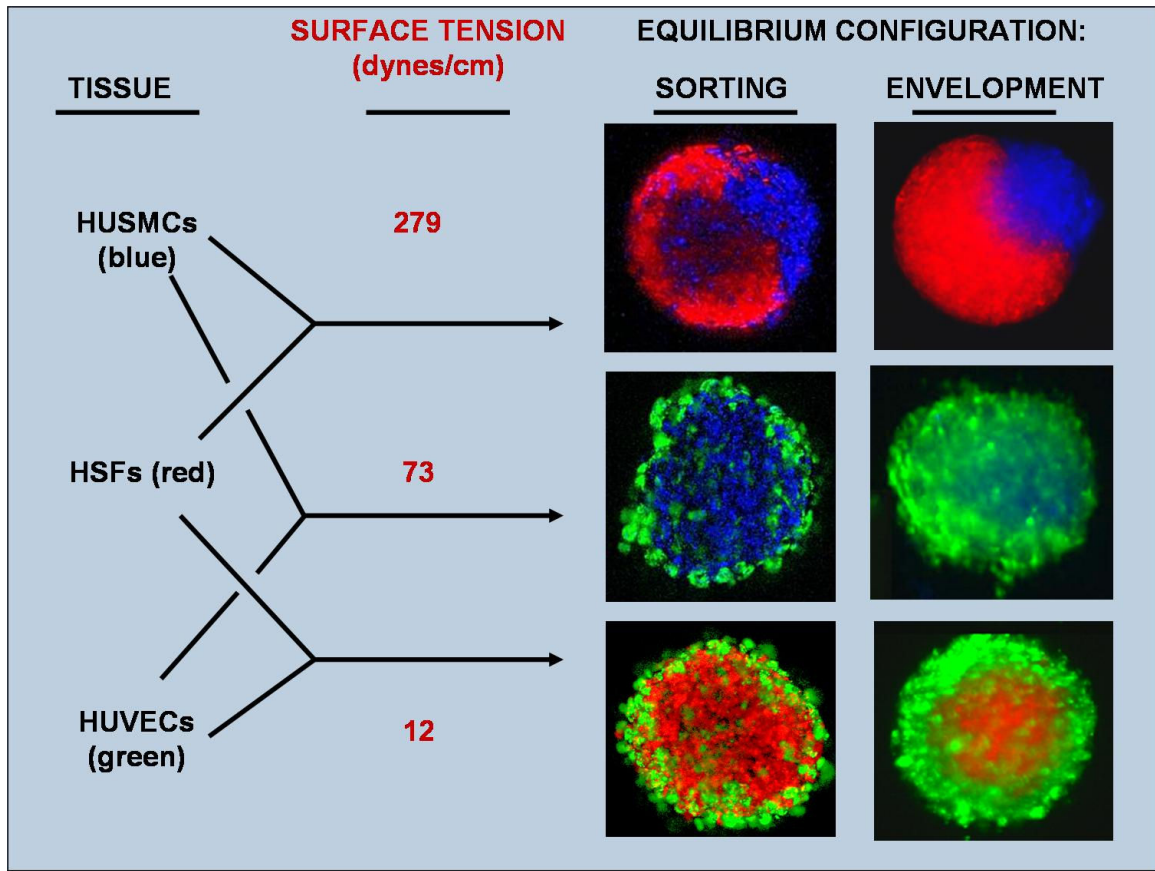


Figure 13. Results of cell segregation assays. The three vascular cell types investigated are shown on the left in the order of their decreasing surface tensions (HUSMC, HSF, HUVEC). On the right are shown equilibrium configurations generated, through cell sorting or envelopment for all possible binary combinations of vascular cell types. Images are 60 μm confocal sections for the sorting experiments, and surface images for spreading experiments. The three vascular cell types were stained with different contrasting fluorescent membrane markers (see Materials and Methods). HUSMCs (blue) are partially enveloped by HSFs (red), which in turn are completely enveloped by HUVECs (green), which in turn, envelop HUVSMCs (blue). In each case, the less cohesive cell types envelops the more cohesive one.

The equilibrium configuration obtained from the sorting or envelopment assays of binary combinations of the three vascular cell types are summarized in Fig. 13: HUVSMCs were partially enveloped by HSFs which, in turn, were enveloped by HUVECs which also

enveloped HUVMSCs. These results indicate that, similarly to immiscible liquids, surface tension guided the segregation of the three main vascular cell types in a transitive manner: HUVECs (the least cohesive cell type) enveloped both HUVMSCs and HSFs, while HUVMSCs (the most cohesive cell types) was enveloped by both HSFs and HUVECs.

The kinetics of segregation assays was quite varied, cell-sorting being a relatively faster process than tissue-spreading. Indeed, HUVECs mixed with either HUVMSCs or HSFs sorted to the surface within 12 hours in both cases and in any environmental condition (gyratory shaker or static agarose bed). By comparison, about 72 hours were needed for the complete envelopment of HSFs or HUVMSCs spheroids by HUVECs spheroids. This difference can probably be explained by two reasons: HUVECs have to move over larger distances in envelopment assays in order to reach an equilibrium configuration, and tissue fusion is an additional time-consuming event as two multicellular spheroids eventually merge into a single one. The time course of segregation patterns for both assays is illustrated in Fig. 14. Interestingly, sorting time for the HUVMSCs-HSFs combination was closer (at least 48 hours) to its respective envelopment time (about 72 hours). In a few cases HSFs sorted into several distinct domains that did not coalesce during the time-course of the experiment.

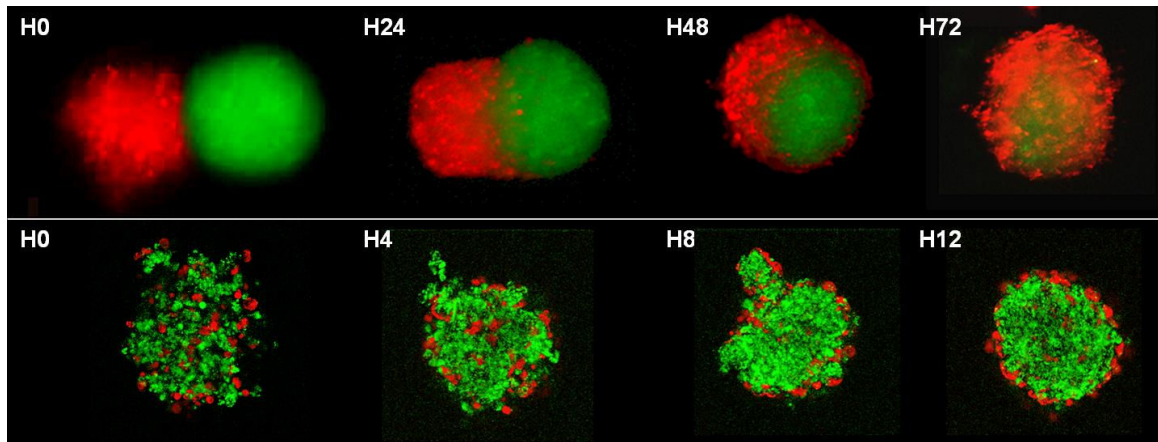


Figure 14. Time-course of envelopment and cell sorting assays. (Top) Multicellular HUVEC spheroid (red) progressively envelops HUVSMC spheroid over the course of 72 hours (left to right). (Bottom) In contrast, cell-sorting is a quicker process, HUVECs enveloping completely HUVSMCs after 12 hours.

We explain this behavior by the relative anatomical complexity of the equilibrium configuration to be reached. Indeed it should be noted that HSFs enveloped HUSMCs only partially (Fig. 13). This means that the cross-adhesions between HSFs and HUVSMCs are weaker than their self-adhesions. For comparison, complete envelopment (HUSMCs-HUVECs and HSFs-HUVECs) corresponds to the case where the cross-adhesions are at least as strong as those between the less cohesive of the two cell populations but not as strong as the average of the two cell populations' individual cohesivities [41]. This relationship between equilibrium configurations and strength of cross-adhesion is illustrated in figure 15.

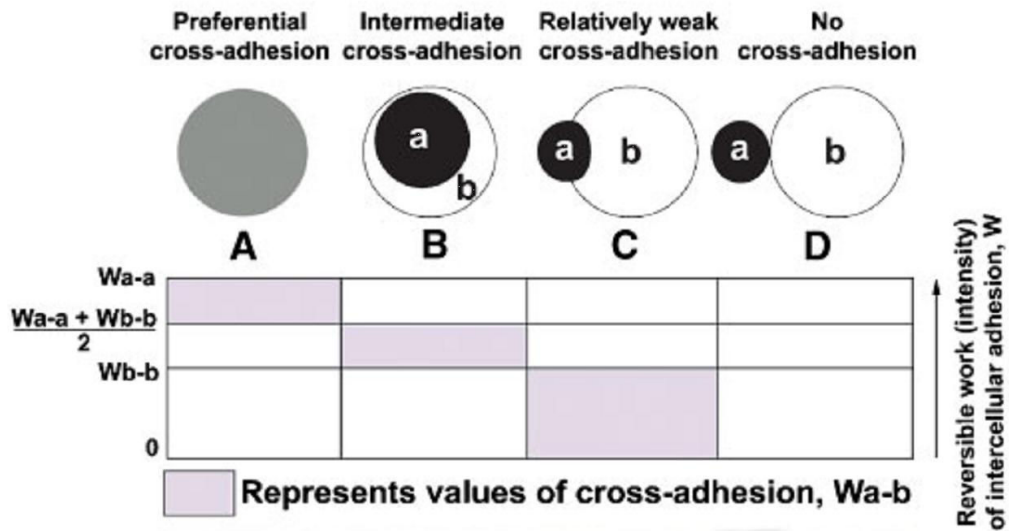


Figure 15. Illustration of how self- (W_{a-a} and W_{b-b}) and cross-adhesions (W_{a-b}) determine the most stable equilibrium configuration. By convention, when the two cell populations differ in cohesiveness, the more cohesive phase is designated a and the less cohesive phase is designated b. In **(A)**, a high degree of cross-adhesion between a and b cell populations results in intermixing. **(D)** represents a situation in which cross-adhesion between the two cell types is minimal. Here, intermixed cells completely sort out from one another, forming two separate spheres. Two mixed cell populations with low but positive values of cross adhesion will lead to partial envelopment **(C)**, while a higher degree of cross-adhesion between the two populations will lead to complete envelopment of one cell population by the other **(B)**. Adapted from [41].

CHAPTER V: DIRECTING MICROTISSUE SELF-ASSEMBLY TOWARDS COMPLEX MACROVASCULAR STRUCTURES

Introduction

In this chapter, we show that multicellular spheroids composed of one or several different vascular cell types can be assembled in precise branched tubular patterns, and that their fusion leads to the formation of custom-shaped multilayered macrovascular structures. More specifically, we report on a novel scaffold-free method for small-diameter blood vessel tissue-engineering. Indeed, vascular grafts are in large demand for coronary and peripheral bypass surgeries. Although synthetic grafts have been developed, replacement of vessels with purely synthetic polymeric conduits often leads to the failure of such graft, especially of grafts with less than 6 mm in diameter or in the areas of low blood flow, mainly due to the early formation of thrombosis. Tissue engineering has become a promising approach for generating a biocompatible vessel graft with growth potential. Since the first success of constructing blood vessels with collagen and cultured vascular cells by Weinberg and Bell (1986) [27], there has been considerable progress in the area of vessel engineering mainly due to the seeding of endothelial cells on the luminal surface in order to provide a non-thrombogenic surface, and the use of biodegradable scaffolds that allow the cells to grow and produce extracellular matrix (ECM) in a three-dimensional environment [121]. However, as we mentioned earlier, the

use of scaffolds has often been associated with chronic inflammation and with impaired tissue remodeling and maturation [28-30].

To address some of afore-mentioned issues, we have recently introduced a novel rapid prototyping technology termed three-dimensional bioprinting, which is based on the automated, computer-aided deposition of “bioink particles” (multicellular spheroids) into a “biopaper” (biocompatible gel; e.g. collagen) [55, 94].

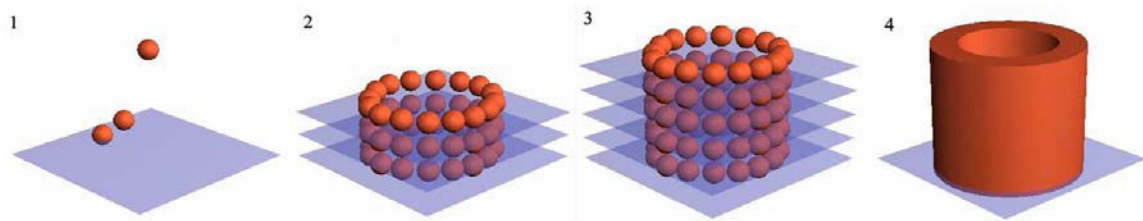


Figure 16. Organ printing concept. Bioink particles (multicellular spheroids) are printed on a biopaper (biocompatible gel) layer by layer until a desired three-dimensional pattern is achieved (1 to 3). Structure formation takes place through the fusion of the bioink particles through the permissive gel which is eventually removed (4). From [122].

Three dimensional tissue structures such as myocardial patches or vascular tubes were formed through the post-printing fusion of the bioink particles similar to self-assembly phenomena in early morphogenesis [123]. Deposition of multicellular spheroids as “bioink” particles with this bioprinting technology was advantageous as it was rapid, precise, assured maximal cell density, while showing minimal cell damage (an effect, often associated with other deposition methods such as ink-jet printing [102, 124]). It is worth noticing that rapid prototyping methods, so far, have focused either on scaffold fabrication or used various hydrogels in combination with cells [125, 126]. As we

reported, the success of the technology depended strongly on the biopaper [55, 93]. Collagen gelation time was critical for the smooth deposition of the multicellular spheroids. Collagen concentration had to be finely tuned in order to assure the fusion of the spheroids during the postprinting phase [93]. Layer-by-layer construction proved to lack precision beyond a few layers due to progressive distortion of the construct, caused by the uneven gelation of successive sheets of biopaper. Biopaper removal after postprinting fusion was technically challenging. It is also reasonable to assume that part of the gel was incorporated in the final tissue structure, as spheroids fuse through the gel. Thus, this method was not completely scaffold-free.

In the present study, we introduce a novel scaffold-free method for small-diameter blood vessel tissue-engineering. To avoid earlier drawbacks associated with the “biopaper” concept, we use agarose gel as a non-adhesive supporting molding element for cellular bioink particle. Structure assembly takes place through the layer-by-layer deposition of convenient units, agarose rods concomitantly with either multicellular spheroids or multicellular cylinders. Biological structures form through the fusion of the cellular spheroids or cylinders. The method allows for precise control of tube geometry such as diameter, wall thickness and branching pattern (Fig. 17). Most importantly, we combine this approach with surface tension-based self-assembly at the microtissue level (as developed in Chapter IV) in order to generate a multilayered vascular wall similar to native blood vessels anatomical organization.

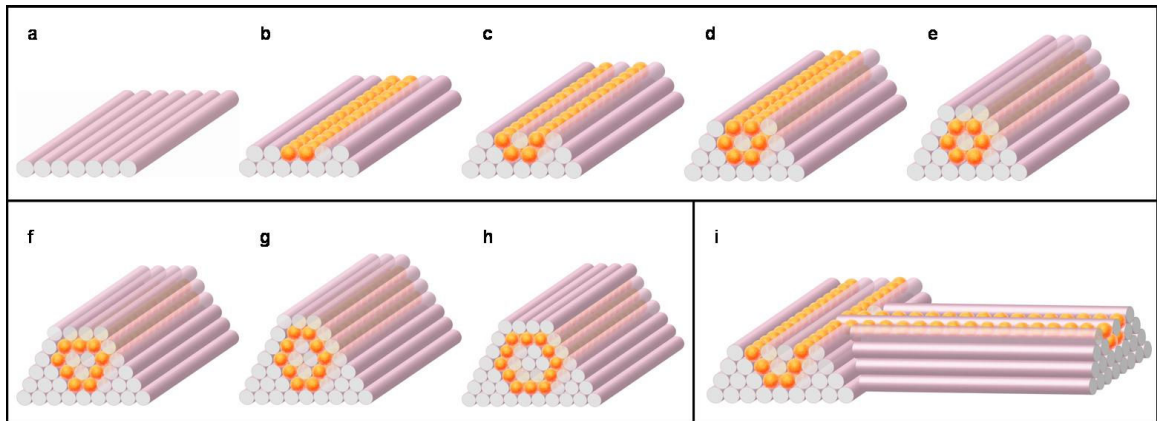


Figure 17. Patterns used for engineering custom-shaped tubular structures. Layer-by-layer deposition of agarose cylinders and multicellular spheroids leads to the assembly of a simple tubular pattern (**a-e**). Construct shape and diameter can be easily adjusted as shown in (**e-h**). Branched tubular structures of distinct diameters are assembled simultaneously in order to allow for continuous lumen (**i**).

We first describe the principles of the method using multicellular spheroids. We then apply these principles to multicellular cylinders to produce single or double-layered tubes composed of SMCs and fibroblasts. We show that this novel scaffold-free method circumvents a number of the shortcomings associated with scaffolds and achieves the goal of being rapid, reproducible, and easily scalable by means of rapid prototyping.

Building scaffold-free, customized macrovascular tubular structures using multicellular spheroids

We first investigated if the novel scaffold-free approach allows the assembly of tissue spheroids into tubular structures of defined topology. To produce multicellular spheroids of specific size we aggregated HUVECs, HUVSMCs, HSFs and CHO cells in

glass micropipettes of 300 or 500 μm . The resulting cylinders were extruded from the micropipettes and cut into equal fragments that were let to round up overnight on a giratory shaker. Depending on the diameter of the micropipettes chosen, this procedure provided regular spheroids of defined size and cell number of (Fig. 10). HUVMSCs and HSFs spheroids displayed similar morphology (Fig. 10 c, d) with smooth and uniform surface and 300 μm spheroids were composed respectively of about 8,000 and 15,000 cells. In contrast, CHO and HUVEC spheroids assumed a berry-like shape (Fig. 10 a, b) suggesting that surface cells adhere more weakly to inner cell layers. The morphological aspects of the surface are indeed consistent with the fact that HUVMSC and HSF spheroids are more cohesive than HUVEC and CHO spheroids as measured by tissue surface tensiometry (see Chapter IV). HUVEC spheroids could not be used in the method detailed below because of their weak self-cohesion ($\sigma = 12$ dynes/cm) (in particular, they naturally dissociated after 2 or 3 days in culture in giratory shaker conditions). In contrast, spheroids composed of a mixture of HUVECs and HSFs, or HUVECs and HUVMSCs, were stable in culture and consequently used in this study.

In order to assemble tissue spheroids into customized tubular structures, we designed a scaffold-free approach based on the use of agarose cylinders as building-blocks of a molding template (Fig. 17). Agarose cylinders were prepared by first loading liquid agarose (temperature $> 40^\circ\text{C}$) into micropipettes (300 or 500 μm ID) and then immersing the micropipettes into cold PBS (4°C). When agarose cylinders and multicellular spheroids of identical size were deposited layer-by-layer (Fig. 17a-e), this template allowed for a precise definition of tube diameter (Fig. 17e-h) and branching pattern (Fig. 17i) with a resolution of a few hundred microns: for example wall thickness

or lumen diameter could be varied with a minimal resolution of 300 μm . Using this approach, straight tubes were initially assembled manually, according to patterns e-h in Fig.17. The smallest tube assembled according to the simplest pattern (Fig. 17e) was 900 μm in diameter with a wall thickness of 300 μm (Fig. 18b).

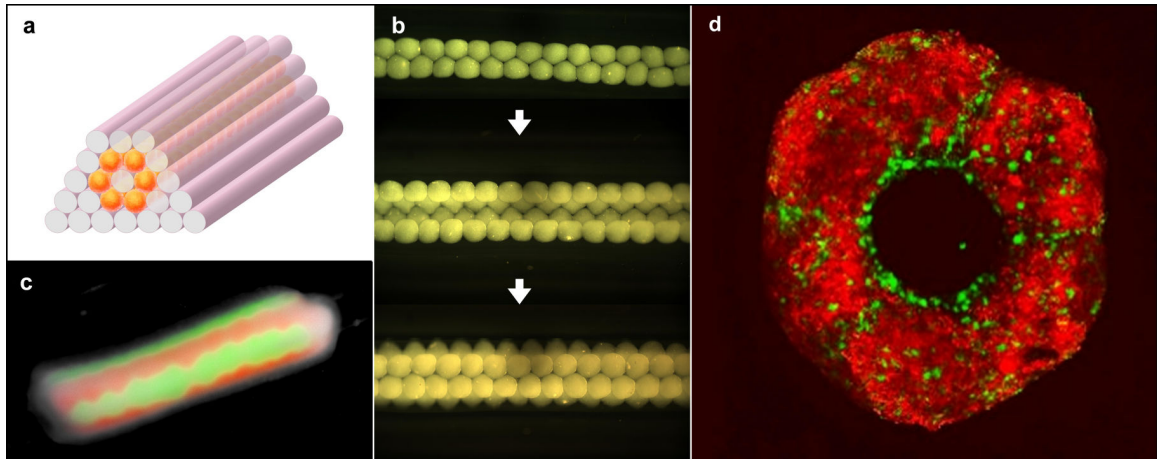


Figure 18. Fusion pattern of various multicellular spheroids assembled into tubular structures. Multicellular spheroids were assembled according to template (a), layer-by-layer as shown in (b) (HSF spheroids). Fusion pattern of a tube assembled from alternate sequences of green and red spheroids of CHO cells is shown in (c) after 7 days. Fusion of spheroids obtained through cell-sorting (HSFs:red; enveloped by HUVECs: green) led to the formation of an endothelial layer around the lumen (d).

Once assembled, multicellular spheroids fused within 5 to 7 days to result in the final tubular construct (Fig 18c). Green and red fluorescent membrane dyes were used in order to study either the fusion pattern between single cell-type spheroids (Fig. 18c), revealing sharp fusion boundaries with little intermingling; or between spheroids composed of mixture of HSFs and HUVECs or HUVSMCs and HUVECs obtained by

cell-sorting (Fig. 14) prior to their assembly in a tubular pattern with this method. Interestingly, in this latter case, the fusion of spheroids that displayed HUVECs on their surface led to the formation of an endothelial layer on the inner surface of the fused tube (Fig. 18d), although some HUVECs failed to migrate on either surface of the tube. This result is important from a tissue-engineering perspective as the presence of an endothelium-lined lumen is essential in preventing thrombogenic events following graft implantation [127]. Importantly, in addition to flexibility in tube diameter and wall thickness, this approach provides a unique way to build branched macrovascular structures. For this purpose, in order to ensure correct luminal connection, the different branches composing the same vascular tree, irrespectively of their diameter, are assembled simultaneously (Fig. 19a). Tubular structures were assembled from various multicellular spheroids with branches of distinct diameters, and fused in 5 to 7 days (Fig. 19 b, c). Despite the relative simplicity of this scaffold-free approach, we noticed several shortcomings, most of them associated with the use of spheroids as building blocks. Indeed, preparation of large quantities of spheroids (> 1000) necessary to build larger and longer tubes is very time-consuming. Also, once assembled into tubular structures, spheroid fusion may take as long as a week and lead to non-uniform tubular surfaces (Fig. 19c). Finally, assembling tubular constructs manually in a sterile fashion, albeit possible (see Materials and Methods), is challenging.

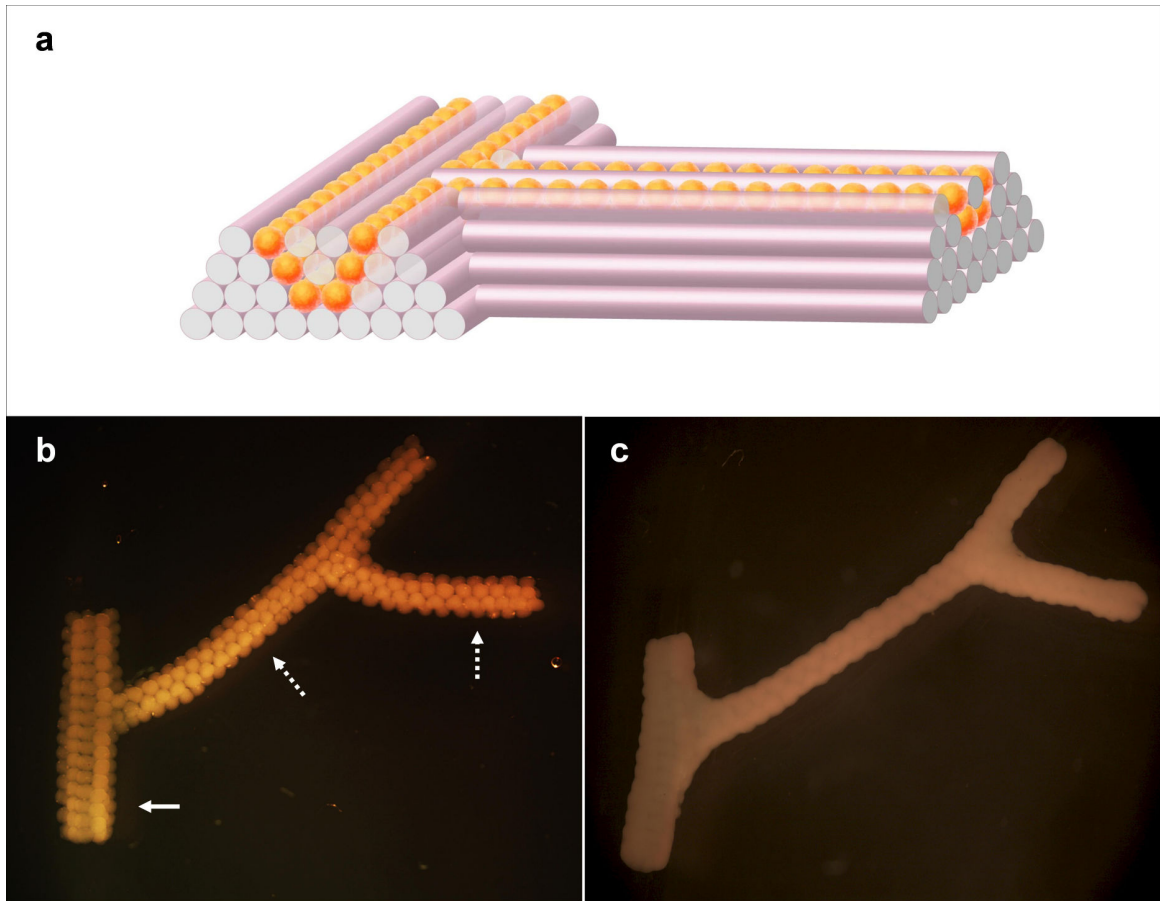


Figure 19. Assembly of a hierarchical vascular tree. Tubular branches of distinct diameters were built from 300 μm HSF spheroids **(b)** which fused within 6 days **(c)**. Connection between the main branch (solid arrow; 1.2 mm OD) and the side branch (dashed arrow; 0.9 mm OD) was achieved according to the template shown in **(a)**.

Using multicellular cylinders as building-blocks for vascular tissue-engineering

Preparation of tubular constructs by the above approach served as proof of principle. We then sought to adapt this method to potential clinical applications, thus to rapid prototyping to gain in speed, precision and reproducibility. For this, we first

investigated whether multicellular cylinders could be used instead of spheroids while keeping the same conceptual approach described above. After cell aggregation into micropipettes, multicellular cylinders were extruded either manually or by an automated deposition process into specifically prepared adhesive-free environment (see Materials and Methods, and Fig. 2). After overnight maturation at 37°C with 5% CO₂, multicellular cylinders were cohesive enough to be printed.

Bioprinting of single and double-layered vascular tubes

The advantage of using cylindrical units, as opposed to spherical ones is that with these “bioink” particles the scheme shown in Fig. 17 can be automated. Indeed, we used a computer-aided rapid prototyping bioprinting technology for the controlled, simultaneous deposition of the agarose rods and multicellular cylinders according to the template shown in Fig. 20 (compare Fig. 17e and Fig. 20a). This was accomplished by special-purpose delivery device with two print heads, one for the preparation and extrusion of agarose rods, the other for the deposition of multicellular cylinder (see Materials and Methods and Fig 20d). Loading, gelation and extrusion of agarose cylinders took place in a fully automatic cycle. The micropipette-cartridge attached to the print head was first moved to a warm 2% liquid agarose vial for loading. Next, to allow for the rapid gelation of agarose, the loaded cartridge was immersed in a cold PBS vial. Finally, the resulting agarose cylinder was extruded into a Petri dish. When the deposition scheme called for the delivery of a multicellular cylinder, one such cylinder was drawn from the agarose

mold into a micropipette. The micropipette was then loaded into the second print head and the cellular cylinder extruded similarly to an agarose cylinder.

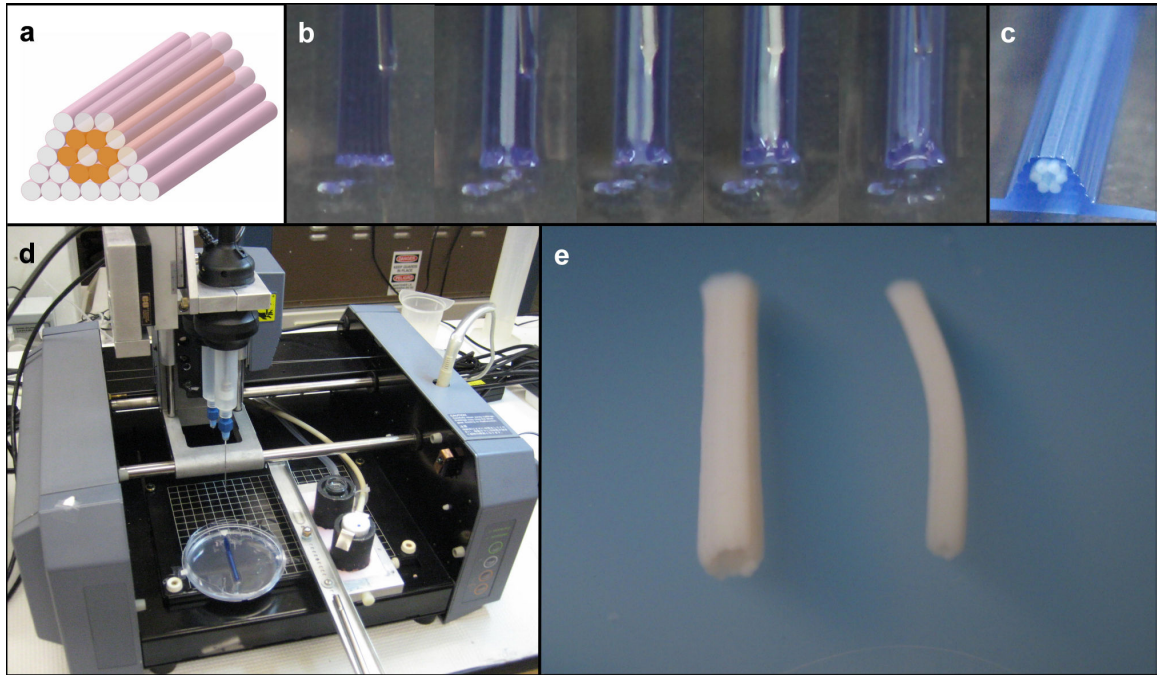


Figure 20. Bioprinting of multicellular cylinders into simple tubular patterns. Tube assembly was achieved (c) through the layer-by-layer deposition (b) of agarose and multicellular PASM cells by a specifically designed bioprinter (d), according to the template shown in (a). Engineered PASM tubes of distinct diameters (left: 2.5 mm OD; right: 1.5 mm OD) are represented after 3 days of fusion (e).

Simple straight tubes of porcine aortic smooth muscle cells (PASCs) were printed according to the design shown in Fig. 20a-c. The computer-aided motion and coordination of the two print heads assured the reproducibility of the pre-programmed pattern (Fig. 20a-c). After assembly, the multicellular cylinders fused within two or three days into the final tubular structure, and the supporting agarose cylinders were manually removed (Fig. 20e).

Next we constructed double-layered vascular tubes similar to vessels in the macrovasculature with a media and adventitia. For this purpose we used both HUSMC and HSF multicellular cylinders as building blocks according to the pattern shown in Fig. 21a.

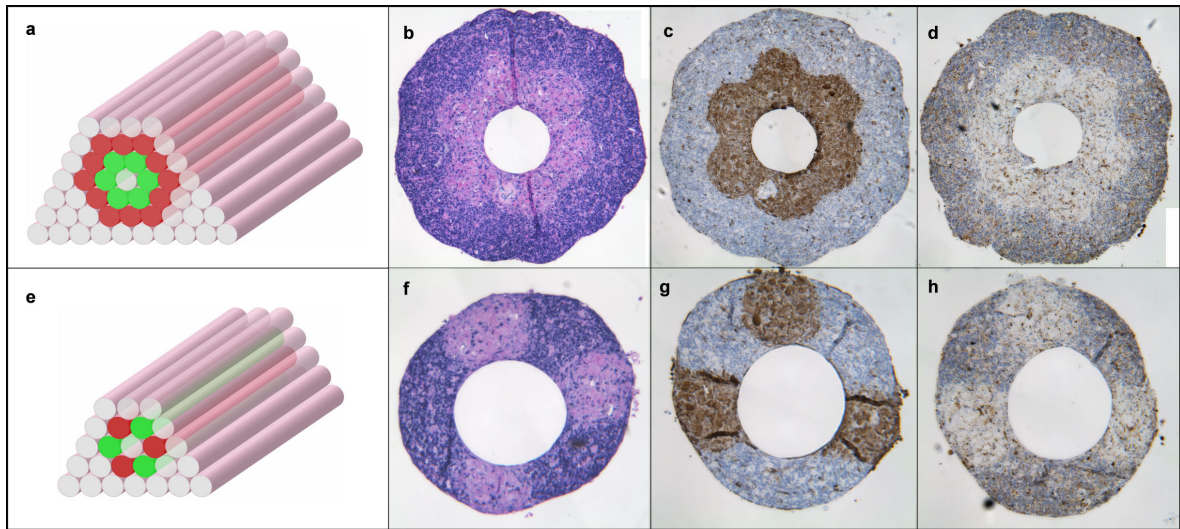


Figure 21. Building a double-layered vascular wall. HUVSMC and HSF multicellular cylinders were assembled according to patterns (a) and (e) (HUVSMCs: green; HSFs: red). Histological examination after 3 days of fusion: HE (b, f), smooth muscle α -actin (brown; c, g) and Caspase-3 (brown; d, h) stainings are shown.

Smooth muscle α -actin staining of HUVSMCs indicated a sharp boundary between the SMC and fibroblast layers in the engineered constructs after 3 days of fusion (Fig. 21c). Caspase-3 staining revealed a few apoptotic cells, sparse throughout the wall (Fig. 21d). To show the versatility of the method, we also engineered tubes by alternatively depositing multicellular cylinders composed of HUVSMCs and HSFs (Fig. 21 e-h), a

pattern that has no in vivo equivalent. Again a clear boundary between the two cell types and limited cell death throughout the wall was observed after three days of fusion (Fig. 21 h, g).

CHAPTER VI: CONCLUSIONS AND PERSPECTIVES

In this work, we have directed the self-assembly of microtissues composed of vascular cells into custom-shaped macrovascular structures using their inherent liquid-like properties and aided by a bioprinting technology. In particular, this work demonstrate the possibility of assembling multilayered tissues composed of different cell types in a novel scaffold-free approach. Another unique aspect of this work concerns the engineering of scaffold-free macrovascular trees, an important aspect for future vascularization of thick tissue-engineered constructs. These conclusions, and others, are further discussed through every specific aim defined in Chapter II.

Specific aim 1

The results presented in Chapter IV confirm that multicellular spheroids composed of any of the three vascular cell types (endothelial cells, fibroblasts, smooth muscle cells) behave like viscous liquids on the long time scale. They are indeed incompressible (Fig. 11) and can be characterized in terms of well-defined apparent surface tension (Fig. 9), smooth muscle cell being the most cohesive cell type ($\sigma = 279$ dynes/cm) and endothelial cell the least cohesive ($\sigma = 12$ dynes/cm). Importantly, since surface tension is a measure of the liquid's cohesivity, in the case of tissues it should be related to molecular parameters. Indeed, it was shown on theoretical grounds that $\sigma \propto JN$, where J and N are, respectively, the bond energy between two homotypic cell adhesion

molecules (CAMs) and the surface number density of CAMs [91]. The linear dependence of the surface tension σ on N has recently been confirmed experimentally by measuring the apparent surface tension of L-cells transfected to express various types of cadherins in varied, measured amounts [64]. However, previous studies have also shown that differential surface contraction and more recently actomyosin-dependent cortical tension can be additional factors implicated in cell sorting and could contribute positively to tissue surface tension [65, 66, 119]. With regard to these two complementary hypotheses, the molecular determinants underlying the extremely high surface tension of smooth muscle cells spheroids (the highest we have ever measured for any cell type) would be interesting to explore further. Indeed, we show that HUVMSCs aggregated in multicellular spheroids express the contractile protein SM α -actin isoform (Fig. 21 c, g), a phenotypic marker usually associated with a mature contractile smooth muscle cell phenotype (other markers include myosin heavy chain and calponin for example) [128]. Also, as we mentioned earlier, the flat surface of HUSMCs spheroids might be representative of a strong cortical tension from surface cells probably combined to a strong adhesion to subsurface layers. Novel methods allowing for the distinct measurement of cortical tension [119, 129] and intercellular adhesion [119, 130, 131] might be able to decipher between the two hypotheses. Another intriguing result concerned the ability of HUVECs, which is an epithelial cell type, arranged in monolayer *in vivo*, to aggregate *in vitro* into three-dimensional spheroids. It is known from *in vivo* models that although VE-cadherin (vascular endothelial cadherin) is mainly involved in mediating adhesion between adjacent endothelial cells, N-cadherin has a mostly dispersed distribution on cell membranes that is excluded to VE-cadherin localization in

most cases [132]. Therefore it would be interesting to explore the expression patterns of these adhesion molecules in three-dimensional endothelial spheroids. More generally, the fact that endothelial cells can be aggregated in three dimensional spheroids can further illustrate a recent interest for this 3D culture method. Indeed, it has been recently demonstrated that multicellular spheroids can serve as *in vitro* 3D models to study epithelial to mesenchymal transition (EMT) in cancer and stem cell research [133, 134]. Although controversial, a few studies support the fact that endothelial cells can transdifferentiate into smooth muscle cells *in vivo*, and *in vitro* in 2D culture [135-139]. Therefore, it would be interesting to explore further this hypothesis using 3D multicellular spheroids as a model for endothelial to mesenchymal (smooth muscle cells and/or fibroblasts) transition. If true, this hypothesis could have important consequences in the field of vascular tissue-engineering as it could provide a unique cell source for all three vascular cell types. The recent discovery of endothelial progenitor cells (EPCs), that can easily be isolated from the peripheral blood [140], is a first step in that direction, as it avoids the surgical harvest of large vessels or tissue microvessels of patients already suffering from vascular disease.

From a physical perspective, surface tension measurement performed on multicellular spheroids led us to solve the Laplace equation for the geometry associated with the equilibrium shape of compressed liquid droplets. In contrast to previous results based on geometrical approximations of the profile of a compressed liquid drop, we show that the exact solution of the Laplace equation allows for a precise determination of σ from a few easily measurable parameters. We have extended this method to the simultaneous compression of several droplets. This is important for gathering statistically

significant data within a short-time frame, as post-compressive equilibration can last up to several hours (depending on the cell type and degree of compression) and surface tension of tissue spheroids can change in time [141]. In addition to confirming that tissues composed of adhesive and motile cells indeed can be characterized in terms of apparent surface tension, we show that compression plate tensiometry can be used to measure the interfacial tension of true liquids, (an application of the method not demonstrated before). As compression plate tensiometry requires minute quantities of liquids it may be more advantageous in case of expensive liquids than classical methods such as the capillary or the De Nouy ring methods.

Specific aim 2

All three vascular cell types displayed segregation behavior through cell-sorting or envelopment assays in agreement with their respective cohesivities or apparent surface tensions. Any binary combination of these cell types led to an equilibrium configuration where the more cohesive cell type (higher surface tension) was surrounded by the less cohesive one (lower surface tension): HUVECs occupied an external position when paired with both HSFs or HUVSMCs, while HUVSMCs occupied an internal position when paired with either HSFs or HUVECs. These results confirm that, similarly to immiscible liquids, surface tension guides the segregation of the three main vascular cell types in a transitive manner. It is difficult not to notice that these in vitro equilibrium configurations are somewhat similar to the anatomical organization of the vascular wall where medial smooth muscle cells are surrounded by both intimal endothelial cells and

adventitial fibroblasts. Although similar in pattern, the vascular wall is very different from these *in vitro* configurations in its composition. In contrast to the multicellular vascular spheroids described in this work, each layer of the vascular wall, in addition to cells, also contains extracellular matrix, such as collagen, elastin and proteoglycans. Thus, it would be erroneous to interpret vascular wall anatomical organization by evoking the liquid analogy, as tissues that contain significant amounts of fibrillar ECM usually display an elastic rather than viscous behavior. Indeed, the explanation for the liquid behavior displayed by a multicellular spheroid stems from the ability of its component cells to slip past each other in response to an applied force (tensiometry compression for example). Although cells are initially stretched, they eventually rearrange to dissipate stresses and viscous behavior dominates at long time scale [117]. Therefore it is very unlikely that any part of the vascular wall, in which cells are deeply entrapped in the ECM, could behave as a viscous liquid.

Specific aim 3

In Chapter V, we show that double-layered tubes can be made using two completely different strategies. First, when placed in a tubular pattern, sorted spheroids composed of HUVECs enveloping either HUVSMCs or HSFs fused to give rise to vascular tubes whose wall is composed of either HSFs or HUVSMCs lined by an endothelial layer on the luminal side (Fig. 18). In the latter case, this organization is similar to small-caliber vessels comporting only two main layers: an intima and a media. Second, multicellular cylinders composed of either HUVSMCs or HSFs were assembled

in a double layer pattern (Fig. 21) and fused to give rise to vascular tubes comporting an outer adventitia-like layer made of HSFs and an inner media-like layer composed of HUVMSCs. The obtained pattern is similar to the anatomical organization of larger vessels. In the latter case, however the endothelial cell layer is missing. Therefore, we have tried to combine both approaches to produce a three-layer vascular tube (data not shown). In that approach, we intended to deposit sorted spheroids composed of HUVECs enveloping HUVMSCs in a tubular pattern, and deposit around it a second layer composed of HSFs spheroids, in a pattern similar to Fig. 21a. When carrying out this program, we encountered serious technical difficulties. When re-ordered, the HUVMSCs and HUVECs cell lines originally used for the tensiometry, aggregation assays, and double-layer tube constructs mentioned above, became senescent in culture, which strongly limited their ability to grow and sort *in vitro*. Both of these cells originated from a cell line collection of unknown passage from ATCC, and every new sample of these cells that we ordered from ATCC failed to grow after about four passages. Interestingly, without further explanation, ATCC recently stopped distributing these cell lines. Therefore, we have recently purchased freshly isolated HUVMSCs and HUVECs from another company (Invitrogen) and are currently repeating these experiments (initial results using these new cell lines confirm that endothelial cells envelop smooth muscle cells in multicellular spheroids through cell-sorting).

In the Introduction, we asked how closely tissue-engineers should try to imitate developmental morphogenesis in order to engineer a given tissue. The present work provides a possible answer to that question. In blood vessel development, typically, vessel wall morphogenesis starts with the formation of a primary vascular network,

composed of nascent endothelial tubes, via the processes of vasculogenesis and angiogenesis. The second step is the recruitment of mural cells that differentiate principally from the mesoderm (with some exceptions). As vascular smooth muscle cells (and later, fibroblasts) become associated with the developing vasculature, they proliferate, produce and organize ECM molecules within the vessel wall, while progressively acquiring a more mature contractile phenotype (for excellent reviews about blood vessel development, see [142, 143]). It is obvious that our approach does not mimic vascular morphogenesis. Instead, we use general developmental processes such as cell-sorting or tissue fusion that are common to the development of many tissues and organs (for a comprehensive review, see [92]). These processes are useful because we do have control over them. In particular, segregation patterns of different vascular cell types can be predicted via tissue surface tension measurement (see Chapter IV), and multilayered tube formation can be achieved through tissue fusion guided by custom-shaped agarose molding templates (see Chapter V). In essence, we take advantage of liquid-like properties of multicellular microtissues and direct their self-assembly in order to create pattern and shape.

Specific aim 4

In Chapter V, we describe a novel approach to build scaffold-free vascular constructs of defined cellular composition and geometry. Linear and branched tubular structures were engineered using various cell types. Parameters such as size, wall thickness or cell patterning were adjusted in order to arrive at single- or double-layered

tubes ranging from 2.5 to 0.9 mm in diameter. Compared to classic scaffold-based approaches, this method avoids a number of the general shortcomings associated with exogenous materials and offers specific advantages. As one example, distributing a high density of cells efficiently and uniformly throughout a scaffold volume remains a significant challenge [144]. In this work, as the engineered constructs are built from cells only, the highest possible cell density is achieved. This is important since, in contrast to cell-sparse tissues such as cartilage, native vessels present a relatively cell-dense media layer with overlapping adjacent SMCs [145]. The presented method relies on building blocks, firm multicellular three-dimensional spheroids or cylinders and thus on the ability of the various cell types, used here, to self-adhere. We have quantified such tissue cohesion through cell-cell interaction by analogy with true liquid systems in Chapter IV, and report that HUVSMCs represent one of the most self-cohesive cell type ever observed [146]. This analogy is exploited through the rounding-up or spontaneous fusion of multicellular spheroids and cylinders described in this work and in earlier tissue-engineering studies [55, 123].

We generated multicellular spheroids using micropipettes of defined diameter (300 μm or 500 μm). Compared to previous approaches for scaffold-free aggregation of cells into spheroids [75, 76, 123], this method provides a reliable way to reproducibly generate spheroids of defined sizes. However the use of tissue spheroids as building blocks had several limitations: (1) the fusion process was long (around one week), (2) and led to a somewhat inhomogeneous construct (Fig. 19); (3) building long vascular tubes was labor- and spheroid-intensive: about 4000 spheroids of 300 μm were needed to fabricate a 10 cm long, 1.5 mm OD tube by the scheme in Fig. 17h. Therefore, we used

of long multicellular cylinders (up to 7cm in length) instead of spheroids which allowed employing the same scaffold-free building concept and improve on the efficacy of fusion.

One current limitation concerns the spatial resolution of the final construct, specifically vascular wall thickness. In this study we used micropipettes of relatively large diameter (300 or 500 μm) for the preparations and deposition of agarose and cellular cylinders. As a consequence, we observed some sparsely distributed apoptotic cells throughout the vascular wall (Fig. 21d, h) after 3 days of fusion. Although, in our case, the apoptotic pattern does not seem to be depth-dependent, it is known that diffusion of nutrients and oxygen is limited to a few hundred microns in vitro engineered tissues [112]. Indeed most tissues need to be vascularized in order to survive, and creating a vascular supply to thick tissue-engineered constructs remains a major challenge [110]. Recently engineering microvascular networks in vitro has become possible, leading to the production of various pre-vascularized bioengineered tissues [113-116]. Despite these advances, viability upon implantation remains problematic because infiltration of surrounding vessels or connection of microvascularized constructs with the host vasculature takes days to weeks, predisposing the tissue to ischemia as the cells wait for a nutrient and oxygen supply to reach them [111]. The ability to create constructs containing a complex hierarchical macro- to micro- vascular tree will be a significant step towards that goal in the sense that this would allow thicker tissues to be perfused *in vitro* for survival and maturation before micro-surgically connecting the macrovasculature of the tissue-engineered construct to the host, as it is commonly done for whole organ transplants. We believe the method presented here is promising also in this respect. To our knowledge, it is the first capable of providing a scaffold-free

hierarchical macro-vascular tree with branching diameter ranging from a few millimeters to under 1 mm (Fig. 19). Due to the current resolution limitations mentioned above, the smallest diameter we can currently achieve is 900 μm OD. However, using smaller micropipettes for the preparation of multicellular cylinder should make it possible to reduce tube diameter to that of arterioles and venules (e.g. using 100 μm micropipettes would lead to 300 μm tubes). At the same time, thinner vascular wall would lead to better viability of cells located in the middle of the wall.

Another issue concerns the removal of the agarose cylinders that occupies the lumen of the branched tubes when the geometry becomes more complex. This is currently achieved by pulling the agarose rods out of the tube manually, procedure that limits the geometry of the final vascular tree: its branches have to be open-ended (Fig. 19). Future studies will investigate the possible use of other molding gels that could be removed by other means (e.g. thermoreversible gels).

Vascular patterning remains a major challenge for small-diameter blood vessel tissue-engineering, mainly due to number and precise position of the vascular cell types within the vascular wall. Small-caliber blood vessels are typically composed of three layers: an inner intima, a thick, dense media, and an outer adventitia, respectively populated by endothelial cells, smooth muscle cells, and fibroblasts. While the inner endothelial monolayer can be quickly achieved by endothelial cell seeding prior to implantation [147], production of a double layered wall that contains a media and an adventitia can be a challenging step in scaffold-based methods [29]. This is due to the difficulty to seed different cell types at precise locations within a single scaffold. Initial positioning of the various cell types is straightforward in the presented method, as

demonstrated by the double-layered tube with its inner and outer layer composed respectively of SMCs and fibroblasts (Fig. 21 a-d), or by the tube with alternative SMC and fibroblast wall segments (Fig. 21 e-h). These results show a unique advantage of this method for precise cell patterning of multiple cell types compared to classic scaffold-based approaches.

Specific aim 5

In Chapter V, we sought to develop a more rapid, high throughput method for engineering vascular tubes, while keeping the same scaffold-free design concept: it involved the use of long multicellular cylinders (up to 7cm in length) instead of spheroids, and implied the use of a rapid prototyping technology, i.e. bioprinting (Fig. 20). A three-dimensional computer-controlled delivery device was used in the different phases of the tube-fabrication process. A microcapillary attachment module (Fig. 2) facilitated the automated, speedy, accurate and simultaneous deposition of ten freshly prepared and still weak multicellular cylinders into the maturation molds (Fig 2 b, d). Overnight maturation of those cylinders in non-adhesive straight grooves of the mold proved to be a critical step in recovering tissue cohesion and preventing any distortion of the cylinders, before their actual layer-by-layer deposition. Post-printing fusion of the cellular cylinders was significantly more rapid (2 to 4 days) and led to the formation of long uniform tubes without any visible macroscopic defaults (Fig. 20e). Overall, compared to tissue spheroids, the use of multicellular cylinders represents considerable progress in terms of time and precision of final structure formation.

Control of geometry and scalability are equally crucial elements for the future development of scaffold-free constructs. In the classic approach, the final geometry of the engineered tissue or organ are controlled by scaffolds of predetermined size and shape [17]. Here we demonstrated that customized scaffold-free vascular tubes may easily be engineered according to a simple design template (Fig. 17). The use of such templates in combination with the rapid-prototyping technology employed assures reliability, accuracy, high throughput, speed and thus potentially easy scalability.

Current and future directions: Maturation of tissue-engineered vessels

Current work focuses on the maturation of the engineered vascular constructs in order to produce the ECM (collagen and elastic fibers) needed to achieve adequate strength and stiffness for implantation in an animal model. Indeed, it is clear that mechanical properties, such as ultimate strength and elasticity, strongly influence short- and long-term patency of vascular grafts used for bypass surgery (for a comprehensive review, see [148]). Studies in several animal species have shown that pulsatile culture conditions promote collagen deposition and alignment and therefore significantly improve mechanical properties of engineered blood vessels [127, 149]. We have therefore designed a bioreactor (see Materials and Methods) in which engineered vascular constructs can be directly perfused with pulsatile flow in order to apply cyclic radial distensions at a controlled frequency and radial strain. Vascular constructs obtained from the fusion of PASMCs multicellular cylinders (see Chapter V) were mounted in the bioreactor and directly perfused with PASMC-specific culture medium under pulsatile

conditions with a radial strain maintained at 5% for a period of 6 weeks at 37°C with 5% CO₂. Histological analysis of matured constructs shows the presence of diffuse collagen on surface layers already by the second week, and circumferentially aligned collagen fibers at 6 weeks in vessels matured in pulsatile conditions (Fig. 22d). In contrast, constructs that were matured in static conditions (still entrapped in agarose molding template) showed fibrillar collagen fibers that were clearly more abundant in surface layers but not as aligned compared to pulsatile condition (Fig. 22e). This difference in collagen amount in the surface layers between pulsatile and static conditions is significant but may have a simple explanation. Indeed it has recently been shown that collagen secreted in soluble form but not cross-linked yet is washed out from cultured cells due to the absence of a confined space typical of real tissues [150]. In pulsatile conditions, this confined space is created by cell proliferation at the surface (Fig. 22b), thus explaining the presence of fibrillar collagen deeper in the construct (Fig. 22d). In contrast, in static conditions, the construct is matured in a confined space (agarose mold) from the start, which could account for the presence of abundant collagen fibers in the more superficial layers (Fig. 22e). Another explanation would attribute this difference to the conditioning of the engineered construct (static vs pulsatile) although we believe it only accounts for differences of organization and alignment of collagen fibers (compare Fig. 22 d and e).

These early results concerning collagen deposition are encouraging although they need to be completed by mechanical testing of matured constructs such as strength and compliance measurements. Indeed collagen is mainly responsible for the ultimate strength of the vascular wall which can be tested through burst pressure. However, Verhoff Van Gieson staining revealed no elastic fibers within the vascular wall after 6

weeks of maturation. This result is not surprising, as producing elastic fibers *in vitro* is still one of the main hurdles of the field [26]. As a consequence engineered vascular grafts are usually poorly compliant.

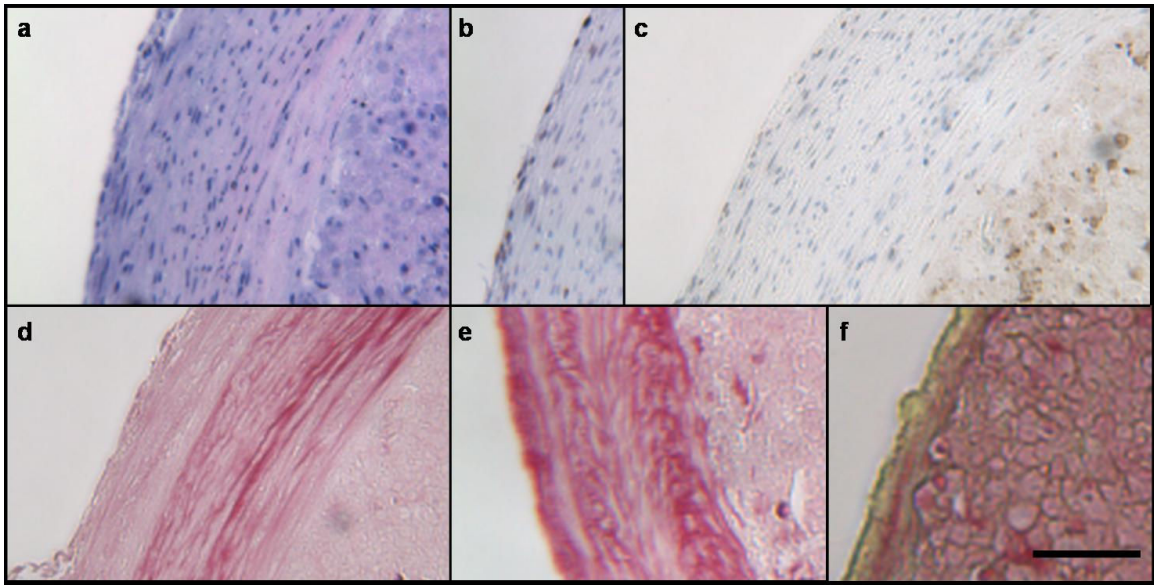


Figure 22. Histological analysis of matured PASMC constructs. (a-c): HE, PCNA (proliferating cells; brown nuclei), and caspase-3 (apoptotic cells; brown) stainings of constructs matured for 6 weeks under pulsatile conditions. Picosirius red stains collagen in constructs matured for 6 weeks under pulsatile conditions (d), or under static conditions after 6 (e) and 2 weeks (f).

The mechanical mismatch between implanted grafts and the adjacent host vasculature typically leads to long-term failure of these graft due to intimal hyperplasia in the anastomotic regions [148]. Another issue concerns viability throughout the construct: although surface cells are circumferentially aligned (Fig. 22a) and mitotically active after 6 weeks (as shown by nuclear staining with Proliferating Cell Nuclear Antigen, Fig. 22b), cells located deeper than 200 μm in the construct are randomly organized and apoptotic (Caspase-3, Fig. 22c). We believe that these apoptotic cells belong in fact to the initial

construct, while collagen-rich surface layers are composed of cells that have proliferated during the maturation period. As we mentioned earlier, it is well known that that nutrients and oxygen diffusion is limited to a few hundred microns in engineered tissues in vitro [112]. This problem is generally not critical for vascular tissue engineering as the vascular wall thickness of small caliber vessels such as coronaries does not exceed a few hundred microns. Therefore, this issue could possibly be circumvented by using smaller diameter multicellular sausages as building blocks for vascular constructs, and by reducing the proliferation rate (by reducing serum concentration in culture medium for example) of surface cells that also contributes to wall thickening. These leads and ideas will be explored in the near future.

REFERENCES

1. Nye, H.L., et al., *Regeneration of the urodele limb: a review*. Dev Dyn, 2003. **226**(2): p. 280-94.
2. Tsonis, P.A., *Regeneration in vertebrates*. Dev Biol, 2000. **221**(2): p. 273-84.
3. Crisan, M., et al., *A perivascular origin for mesenchymal stem cells in multiple human organs*. Cell Stem Cell, 2008. **3**(3): p. 301-13.
4. Pittenger, M.F., et al., *Multilineage potential of adult human mesenchymal stem cells*. Science, 1999. **284**(5411): p. 143-7.
5. Odorico, J.S., D.S. Kaufman, and J.A. Thomson, *Multilineage differentiation from human embryonic stem cell lines*. Stem Cells, 2001. **19**(3): p. 193-204.
6. Takahashi, K., et al., *Induction of pluripotent stem cells from adult human fibroblasts by defined factors*. Cell, 2007. **131**(5): p. 861-72.
7. Yu, J., et al., *Induced pluripotent stem cell lines derived from human somatic cells*. Science, 2007. **318**(5858): p. 1917-20.
8. Mooney, D.J. and H. Vandenburgh, *Cell delivery mechanisms for tissue repair*. Cell Stem Cell, 2008. **2**(3): p. 205-13.
9. Griffith, L.G. and G. Naughton, *Tissue engineering--current challenges and expanding opportunities*. Science, 2002. **295**(5557): p. 1009-14.
10. Langer, R. and J.P. Vacanti, *Tissue engineering*. Science, 1993. **260**(5110): p. 920-6.
11. Grayson, W.L., et al., *Biomimetic approach to tissue engineering*. Semin Cell Dev Biol, 2008.
12. Ingber, D.E., et al., *Tissue engineering and developmental biology: going biomimetic*. Tissue Eng, 2006. **12**(12): p. 3265-83.
13. Roell, W., et al., *Engraftment of connexin 43-expressing cells prevents post-infarct arrhythmia*. Nature, 2007. **450**(7171): p. 819-24.
14. McKee, J.A., et al., *Human arteries engineered in vitro*. EMBO Rep, 2003. **4**(6): p. 633-8.

15. Hutmacher, D.W., *Scaffold design and fabrication technologies for engineering tissues--state of the art and future perspectives*. J Biomater Sci Polym Ed, 2001. **12**(1): p. 107-24.
16. Vacanti, J.P., et al., *Selective cell transplantation using bioabsorbable artificial polymers as matrices*. J Pediatr Surg, 1988. **23**(1 Pt 2): p. 3-9.
17. Cao, Y., et al., *Transplantation of chondrocytes utilizing a polymer-cell construct to produce tissue-engineered cartilage in the shape of a human ear*. Plast Reconstr Surg, 1997. **100**(2): p. 297-302; discussion 303-4.
18. Lee, K., et al., *Cell therapy for bone regeneration-Bench to bedside*. J Biomed Mater Res B Appl Biomater, 2008.
19. Kerker, J.T., A.J. Leo, and N.A. Sgaglione, *Cartilage repair: synthetics and scaffolds: basic science, surgical techniques, and clinical outcomes*. Sports Med Arthrosc, 2008. **16**(4): p. 208-16.
20. van Tienen, T.G., G. Hannink, and P. Buma, *Meniscus replacement using synthetic materials*. Clin Sports Med, 2009. **28**(1): p. 143-56.
21. Atala, A., et al., *Tissue-engineered autologous bladders for patients needing cystoplasty*. Lancet, 2006. **367**(9518): p. 1241-6.
22. Priya, S.G., H. Jungvid, and A. Kumar, *Skin tissue engineering for tissue repair and regeneration*. Tissue Eng Part B Rev, 2008. **14**(1): p. 105-18.
23. Williams, D.F., *On the mechanisms of biocompatibility*. Biomaterials, 2008. **29**(20): p. 2941-53.
24. Shimizu, T., et al., *Cell sheet engineering for myocardial tissue reconstruction*. Biomaterials, 2003. **24**(13): p. 2309-16.
25. Zimmermann, W.H., et al., *Heart muscle engineering: an update on cardiac muscle replacement therapy*. Cardiovasc Res, 2006. **71**(3): p. 419-29.
26. Patel, A., et al., *Elastin biosynthesis: The missing link in tissue-engineered blood vessels*. Cardiovasc Res, 2006. **71**(1): p. 40-9.
27. Weinberg, C.B. and E. Bell, *A blood vessel model constructed from collagen and cultured vascular cells*. Science, 1986. **231**(4736): p. 397-400.
28. Dahl, S.L., et al., *Mechanical properties and compositions of tissue engineered and native arteries*. Ann Biomed Eng, 2007. **35**(3): p. 348-55.
29. Iwasaki, K., et al., *Bioengineered three-layered robust and elastic artery using hemodynamically-equivalent pulsatile bioreactor*. Circulation, 2008. **118**(14 Suppl): p. S52-7.

30. Higgins, S.P., A.K. Solan, and L.E. Niklason, *Effects of polyglycolic acid on porcine smooth muscle cell growth and differentiation*. J Biomed Mater Res A, 2003. **67**(1): p. 295-302.
31. Shin'oka, T., Y. Imai, and Y. Ikada, *Transplantation of a tissue-engineered pulmonary artery*. N Engl J Med, 2001. **344**(7): p. 532-3.
32. L'Heureux, N., et al., *A completely biological tissue-engineered human blood vessel*. Faseb J, 1998. **12**(1): p. 47-56.
33. L'Heureux, N., T.N. McAllister, and L.M. de la Fuente, *Tissue-engineered blood vessel for adult arterial revascularization*. N Engl J Med, 2007. **357**(14): p. 1451-3.
34. Masuda, S., et al., *Cell sheet engineering for heart tissue repair*. Adv Drug Deliv Rev, 2008. **60**(2): p. 277-85.
35. Newman, S.A. and R. Bhat, *Dynamical patterning modules: physico-genetic determinants of morphological development and evolution*. Phys Biol, 2008. **5**(1): p. 15008.
36. Forgacs, G. and S.A. Newman, *Biological Physics of the Developing Embryo*. 2005: Cambridge University Press.
37. Steinberg, M.S. and T. Poole, *Liquid behavior of embryonic tissues*, in *Cell behavior*. 1982, Cambridge University Press. p. pp 583-607.
38. Armstrong, P.B., *Cell sorting out: the self-assembly of tissues in vitro*. Crit Rev Biochem Mol Biol, 1989. **24**(2): p. 119-49.
39. Beysens, D.A., G. Forgacs, and J.A. Glazier, *Cell sorting is analogous to phase ordering in fluids*. Proc Natl Acad Sci U S A, 2000. **97**(17): p. 9467-71.
40. Flenner, E., et al., *Relating biophysical properties across scales*. Curr Top Dev Biol, 2008. **81**: p. 461-83.
41. Foty, R.A. and M.S. Steinberg, *Cadherin-mediated cell-cell adhesion and tissue segregation in relation to malignancy*. Int J Dev Biol, 2004. **48**(5-6): p. 397-409.
42. Lecuit, T. and P.F. Lenne, *Cell surface mechanics and the control of cell shape, tissue patterns and morphogenesis*. Nat Rev Mol Cell Biol, 2007. **8**(8): p. 633-44.
43. Davis, G.S., H.M. Phillips, and M.S. Steinberg, *Germ-layer surface tensions and "tissue affinities" in Rana pipiens gastrulae: quantitative measurements*. Dev Biol, 1997. **192**(2): p. 630-44.

44. Damon, B.J., et al., *Limb bud and flank mesoderm have distinct "physical phenotypes" that may contribute to limb budding*. Dev Biol, 2008. **321**(2): p. 319-30.
45. Heintzelman, K.F., H.M. Phillips, and G.S. Davis, *Liquid-tissue behavior and differential cohesiveness during chick limb budding*. J Embryol Exp Morphol, 1978. **47**: p. 1-15.
46. Israelachvili, J., *Intermolecular and Surface Forces*. 1992, New York: Academic Press.
47. Steinberg, M.S., *On the mechanism of tissue reconstruction by dissociated cells. I. Population kinetics, differential adhesiveness. and the absence of directed migration*. Proc Natl Acad Sci U S A, 1962. **48**: p. 1577-82.
48. Steinberg, M.S., *Mechanism of tissue reconstruction by dissociated cells. II. Time-course of events*. Science, 1962. **137**: p. 762-3.
49. Steinberg, M.S., *On the Mechanism of Tissue Reconstruction by Dissociated Cells, Iii. Free Energy Relations and the Reorganization of Fused, Heteronomic Tissue Fragments*. Proc Natl Acad Sci U S A, 1962. **48**(10): p. 1769-76.
50. Steinberg, M.S., *Reconstruction of tissues by dissociated cells. Some morphogenetic tissue movements and the sorting out of embryonic cells may have a common explanation*. Science, 1963. **141**: p. 401-8.
51. Steinberg, M.S. and S.A. Roth, *Phases in Cell Aggregation and Tissue Reconstruction an Approach to the Kinetics of Cell Aggregation*. J Exp Zool, 1964. **157**: p. 327-38.
52. Steinberg, M.S., *Does differential adhesion govern self-assembly processes in histogenesis? Equilibrium configurations and the emergence of a hierarchy among populations of embryonic cells*. J Exp Zool, 1970. **173**(4): p. 395-433.
53. Holtfreter, j., *Gewebeaffinität, ein Mittel der embryonal Formbildung*. Arch. Exptl. Zellforsch. Gewebezucht., 1939(23): p. 169-209.
54. Townes, p. and j. Holtfreter, *Directed movements and selective adhesion of embryonic amphibian cells*. J. Exptl. Zool., 1955(128): p. 53-120.
55. Jakab, K., et al., *Tissue engineering by self-assembly of cells printed into topologically defined structures*. Tissue Eng Part A, 2008. **14**(3): p. 413-21.
56. Jakab, K., et al., *Relating cell and tissue mechanics: implications and applications*. Dev Dyn, 2008. **237**(9): p. 2438-49.
57. Armstrong, P.B., *Modulation of tissue affinities of cardiac myocyte aggregates by mesenchyme*. Dev Biol, 1978. **64**(1): p. 60-72.

58. Torza, S. and S.G. Mason, *Coalescence of Two Immiscible Liquid Drops*. Science, 1969. **163**(3869): p. 813-814.
59. Foty, R.A., et al., *Liquid properties of embryonic tissues: Measurement of interfacial tensions*. Phys Rev Lett, 1994. **72**(14): p. 2298-2301.
60. Foty, R.A., et al., *Surface tensions of embryonic tissues predict their mutual envelopment behavior*. Development, 1996. **122**(5): p. 1611-20.
61. Duguay, D., R.A. Foty, and M.S. Steinberg, *Cadherin-mediated cell adhesion and tissue segregation: qualitative and quantitative determinants*. Dev Biol, 2003. **253**(2): p. 309-23.
62. Steinberg, M.S. and M. Takeichi, *Experimental specification of cell sorting, tissue spreading, and specific spatial patterning by quantitative differences in cadherin expression*. Proc Natl Acad Sci U S A, 1994. **91**(1): p. 206-9.
63. Hayashi, T. and R.W. Carthew, *Surface mechanics mediate pattern formation in the developing retina*. Nature, 2004. **431**(7009): p. 647-52.
64. Foty, R.A. and M.S. Steinberg, *The differential adhesion hypothesis: a direct evaluation*. Dev Biol, 2005. **278**(1): p. 255-63.
65. Harris, A., *Is cell sorting caused by differences in the work of intercellular adhesion? A critique of the Steinberg Hypothesis*. J. Theor. Biol., 1975(61): p. 267-285.
66. Brodland, G.W., *The Differential Interfacial Tension Hypothesis (DITH): a comprehensive theory for the self-rearrangement of embryonic cells and tissues*. J Biomech Eng, 2002. **124**(2): p. 188-97.
67. Rauzi, M., et al., *Nature and anisotropy of cortical forces orienting Drosophila tissue morphogenesis*. Nat Cell Biol, 2008. **10**(12): p. 1401-10.
68. Kafer, J., et al., *Cell adhesion and cortex contractility determine cell patterning in the Drosophila retina*. Proc Natl Acad Sci U S A, 2007. **104**(47): p. 18549-54.
69. Moscona, A. and H. Moscona, *The dissociation and aggregation of cells from organ rudiments of the early chick embryo*. J Anat, 1952. **86**(3): p. 287-301.
70. Weiss, P. and A. Moscona, *Type-specific morphogenesis of cartilages developed from dissociated limb and scleral mesenchyme in vitro*. J Embryol Exp Morphol, 1958. **6**(2): p. 238-46.
71. Moscona, A.A., *Tissues from dissociated cells*. Sci Am, 1959. **200**(5): p. 132-4 passim.

72. Weiss, P. and A.C. Taylor, *Reconstitution of Complete Organs from Single-Cell Suspensions of Chick Embryos in Advanced Stages of Differentiation*. Proc Natl Acad Sci U S A, 1960. **46**(9): p. 1177-85.
73. Holtfreter, j., *A study of the mechanisms of gastrulation*. J. Exptl. Zool., 1944(95): p. 171-212.
74. Napolitano, A.P., et al., *Dynamics of the self-assembly of complex cellular aggregates on micromolded nonadhesive hydrogels*. Tissue Eng, 2007. **13**(8): p. 2087-94.
75. Lin, R.Z. and H.Y. Chang, *Recent advances in three-dimensional multicellular spheroid culture for biomedical research*. Biotechnol J, 2008. **3**(9-10): p. 1172-84.
76. Kelm, J.M. and M. Fussenegger, *Microscale tissue engineering using gravity-enforced cell assembly*. Trends Biotechnol, 2004. **22**(4): p. 195-202.
77. Friedrich, J., R. Ebner, and L.A. Kunz-Schughart, *Experimental anti-tumor therapy in 3-D: spheroids--old hat or new challenge?* Int J Radiat Biol, 2007. **83**(11-12): p. 849-71.
78. Kloss, D., et al., *Drug testing on 3D in vitro tissues trapped on a microcavity chip*. Lab Chip, 2008. **8**(6): p. 879-84.
79. Kunz-Schughart, L.A., et al., *The use of 3-D cultures for high-throughput screening: the multicellular spheroid model*. J Biomol Screen, 2004. **9**(4): p. 273-85.
80. Mueller-Klieser, W., *Three-dimensional cell cultures: from molecular mechanisms to clinical applications*. Am J Physiol, 1997. **273**(4 Pt 1): p. C1109-23.
81. Winters, B.S., et al., *Three-dimensional culture regulates Raf-1 expression to modulate fibronectin matrix assembly*. Mol Biol Cell, 2006. **17**(8): p. 3386-96.
82. Abu-Absi, S.F., et al., *Structural polarity and functional bile canaliculi in rat hepatocyte spheroids*. Exp Cell Res, 2002. **274**(1): p. 56-67.
83. Landry, J., et al., *Spheroidal aggregate culture of rat liver cells: histotypic reorganization, biomatrix deposition, and maintenance of functional activities*. J Cell Biol, 1985. **101**(3): p. 914-23.
84. Matta, S.G., et al., *Pancreatic islet cell reaggregation systems: efficiency of cell reassociation and endocrine cell topography of rat islet-like aggregates*. Pancreas, 1994. **9**(4): p. 439-49.

85. Korff, T. and H.G. Augustin, *Integration of endothelial cells in multicellular spheroids prevents apoptosis and induces differentiation*. J Cell Biol, 1998. **143**(5): p. 1341-52.
86. Gentile, C., et al., *VEGF-mediated fusion in the generation of uniluminal vascular spheroids*. Dev Dyn, 2008. **237**(10): p. 2918-25.
87. Kelm, J.M., et al., *Method for generation of homogeneous multicellular tumor spheroids applicable to a wide variety of cell types*. Biotechnol Bioeng, 2003. **83**(2): p. 173-80.
88. Akiyama, M., et al., *Periosteal cell pellet culture system: a new technique for bone engineering*. Cell Transplant, 2006. **15**(6): p. 521-32.
89. Korff, T., et al., *Blood vessel maturation in a 3-dimensional spheroidal coculture model: direct contact with smooth muscle cells regulates endothelial cell quiescence and abrogates VEGF responsiveness*. Faseb J, 2001. **15**(2): p. 447-57.
90. Jia, D., D. Dajusta, and R.A. Foty, *Tissue surface tensions guide in vitro self-assembly of rodent pancreatic islet cells*. Dev Dyn, 2007. **236**(8): p. 2039-49.
91. Forgacs, G., et al., *Viscoelastic properties of living embryonic tissues: a quantitative study*. Biophys J, 1998. **74**(5): p. 2227-34.
92. Perez-Pomares, J.M. and R.A. Foty, *Tissue fusion and cell sorting in embryonic development and disease: biomedical implications*. Bioessays, 2006. **28**(8): p. 809-21.
93. Jakab, K., et al., *Engineering biological structures of prescribed shape using self-assembling multicellular systems*. Proc Natl Acad Sci U S A, 2004. **101**(9): p. 2864-9.
94. Neagu, A., et al., *Role of physical mechanisms in biological self-organization*. Phys Rev Lett, 2005. **95**(17): p. 178104.
95. Perez-Pomares, J.M., et al., *In vitro self-assembly of proepicardial cell aggregates: an embryonic vasculogenic model for vascular tissue engineering*. Anat Rec A Discov Mol Cell Evol Biol, 2006. **288**(7): p. 700-13.
96. Rago, A.P., D.M. Dean, and J.R. Morgan, *Controlling cell position in complex heterotypic 3D microtissues by tissue fusion*. Biotechnol Bioeng, 2009. **102**(4): p. 1231-41.
97. Kelm, J.M., et al., *Design of custom-shaped vascularized tissues using microtissue spheroids as minimal building units*. Tissue Eng, 2006. **12**(8): p. 2151-60.

98. Mironov, V., et al., *Organ printing: promises and challenges*. Regen Med, 2008. **3**(1): p. 93-103.
99. Jakab, K., et al., *Organ printing: fiction or science*. Biorheology, 2004. **41**(3-4): p. 371-5.
100. Sun, W., et al., *Computer-aided tissue engineering: overview, scope and challenges*. Biotechnol Appl Biochem, 2004. **39**(Pt 1): p. 29-47.
101. Xu, T., et al., *Inkjet printing of viable mammalian cells*. Biomaterials, 2005. **26**(1): p. 93-9.
102. Boland, T., et al., *Application of inkjet printing to tissue engineering*. Biotechnol J, 2006. **1**(9): p. 910-7.
103. Kelm, J.M., et al., *In vitro vascularization of human connective microtissues*. Methods Mol Med, 2007. **140**: p. 153-66.
104. Kunz-Schughart, L.A., et al., *Potential of fibroblasts to regulate the formation of three-dimensional vessel-like structures from endothelial cells in vitro*. Am J Physiol Cell Physiol, 2006. **290**(5): p. C1385-98.
105. Sapsford, R.N., G.D. Oakley, and S. Talbot, *Early and late patency of expanded polytetrafluoroethylene vascular grafts in aorta-coronary bypass*. J Thorac Cardiovasc Surg, 1981. **81**(6): p. 860-4.
106. Greisler, H.P., *Interactions at the blood/material interface*. Ann Vasc Surg, 1990. **4**(1): p. 98-103.
107. Thom, T., et al., *Heart disease and stroke statistics--2006 update: a report from the American Heart Association Statistics Committee and Stroke Statistics Subcommittee*. Circulation, 2006. **113**(6): p. e85-151.
108. Conte, M.S., *The ideal small arterial substitute: a search for the Holy Grail?* Faseb J, 1998. **12**(1): p. 43-5.
109. Greenwald, S.E. and C.L. Berry, *Improving vascular grafts: the importance of mechanical and haemodynamic properties*. J Pathol, 2000. **190**(3): p. 292-9.
110. Ko, H.C., B.K. Milthorpe, and C.D. McFarland, *Engineering thick tissues--the vascularisation problem*. Eur Cell Mater, 2007. **14**: p. 1-18; discussion 18-9.
111. Rouwkema, J., N.C. Rivron, and C.A. van Blitterswijk, *Vascularization in tissue engineering*. Trends Biotechnol, 2008. **26**(8): p. 434-41.
112. Muschler, G.F., C. Nakamoto, and L.G. Griffith, *Engineering principles of clinical cell-based tissue engineering*. J Bone Joint Surg Am, 2004. **86-A**(7): p. 1541-58.

113. Black, A.F., et al., *In vitro reconstruction of a human capillary-like network in a tissue-engineered skin equivalent*. *Faseb J*, 1998. **12**(13): p. 1331-40.
114. Unger, R.E., et al., *Tissue-like self-assembly in cocultures of endothelial cells and osteoblasts and the formation of microcapillary-like structures on three-dimensional porous biomaterials*. *Biomaterials*, 2007. **28**(27): p. 3965-76.
115. Levenberg, S., et al., *Engineering vascularized skeletal muscle tissue*. *Nat Biotechnol*, 2005. **23**(7): p. 879-84.
116. Caspi, O., et al., *Tissue engineering of vascularized cardiac muscle from human embryonic stem cells*. *Circ Res*, 2007. **100**(2): p. 263-72.
117. Phillips, H.M., M.S. Steinberg, and B.H. Lipton, *Embryonic tissues as elasticoviscous liquids. II. Direct evidence for cell slippage in centrifuged aggregates*. *Dev Biol*, 1977. **59**(2): p. 124-34.
118. Cai, X., *Regulation of smooth muscle cells in development and vascular disease: current therapeutic strategies*. *Expert Rev Cardiovasc Ther*, 2006. **4**(6): p. 789-800.
119. Krieg, M., et al., *Tensile forces govern germ-layer organization in zebrafish*. *Nat Cell Biol*, 2008. **10**(4): p. 429-36.
120. Phillips, H.M. and G.S. Davis, *Liquid-tissue mechanics in amphibian gastrulation: germ layer assembly in *Rana pipiens**. *Amer. Zool.*, 1978(18): p. 81-93.
121. Niklason, L.E., et al., *Functional arteries grown in vitro*. *Science*, 1999. **284**(5413): p. 489-93.
122. Jakab, K., *Physical mechanisms of cell rearrangements: from tissue liquidity to artificial organ structures*, in *Department of Physics and Astronomy*. 2006, University of Missouri: Columbia. p. 76.
123. Marga, F., et al., *Developmental biology and tissue engineering*. *Birth Defects Res C Embryo Today*, 2007. **81**(4): p. 320-8.
124. Mironov, V., N. Reis, and B. Derby, *Review: bioprinting: a beginning*. *Tissue Eng*, 2006. **12**(4): p. 631-4.
125. Fedorovich, N.E., et al., *Hydrogels as extracellular matrices for skeletal tissue engineering: state-of-the-art and novel application in organ printing*. *Tissue Eng*, 2007. **13**(8): p. 1905-25.
126. Yang, S., et al., *The design of scaffolds for use in tissue engineering. Part II. Rapid prototyping techniques*. *Tissue Eng*, 2002. **8**(1): p. 1-11.

127. Isenberg, B.C., C. Williams, and R.T. Tranquillo, *Small-diameter artificial arteries engineered in vitro*. *Circ Res*, 2006. **98**(1): p. 25-35.
128. Owens, G.K., M.S. Kumar, and B.R. Wamhoff, *Molecular regulation of vascular smooth muscle cell differentiation in development and disease*. *Physiol Rev*, 2004. **84**(3): p. 767-801.
129. Evans, E. and A. Yeung, *Apparent viscosity and cortical tension of blood granulocytes determined by micropipet aspiration*. *Biophys J*, 1989. **56**(1): p. 151-60.
130. Puech, P.H., et al., *A new technical approach to quantify cell-cell adhesion forces by AFM*. *Ultramicroscopy*, 2006. **106**(8-9): p. 637-44.
131. Zhang, X., et al., *Atomic force microscopy measurement of leukocyte-endothelial interaction*. *Am J Physiol Heart Circ Physiol*, 2004. **286**(1): p. H359-67.
132. Nyqvist, D., C. Giampietro, and E. Dejana, *Deciphering the functional role of endothelial junctions by using in vivo models*. *EMBO Rep*, 2008. **9**(8): p. 742-7.
133. Chu, J.H., et al., *Development of a three-dimensional culture model of prostatic epithelial cells and its use for the study of epithelial-mesenchymal transition and inhibition of PI3K pathway in prostate cancer*. *Prostate*, 2009. **69**(4): p. 428-42.
134. Mani, S.A., et al., *The epithelial-mesenchymal transition generates cells with properties of stem cells*. *Cell*, 2008. **133**(4): p. 704-15.
135. Frid, M.G., V.A. Kale, and K.R. Stenmark, *Mature vascular endothelium can give rise to smooth muscle cells via endothelial-mesenchymal transdifferentiation: in vitro analysis*. *Circ Res*, 2002. **90**(11): p. 1189-96.
136. DeRuiter, M.C., et al., *Embryonic endothelial cells transdifferentiate into mesenchymal cells expressing smooth muscle actins in vivo and in vitro*. *Circ Res*, 1997. **80**(4): p. 444-51.
137. Zeisberg, E.M., et al., *Fibroblasts in kidney fibrosis emerge via endothelial-to-mesenchymal transition*. *J Am Soc Nephrol*, 2008. **19**(12): p. 2282-7.
138. Zeisberg, E.M., et al., *Discovery of endothelial to mesenchymal transition as a source for carcinoma-associated fibroblasts*. *Cancer Res*, 2007. **67**(21): p. 10123-8.
139. Arciniegas, E., et al., *Transforming growth factor beta 1 promotes the differentiation of endothelial cells into smooth muscle-like cells in vitro*. *J Cell Sci*, 1992. **103** (Pt 2): p. 521-9.
140. Asahara, T., et al., *Isolation of putative progenitor endothelial cells for angiogenesis*. *Science*, 1997. **275**(5302): p. 964-7.

141. Robinson, E.E., et al., *Alpha5beta1 integrin mediates strong tissue cohesion*. J Cell Sci, 2003. **116**(Pt 2): p. 377-86.
142. Drake, C.J., J.E. Hungerford, and C.D. Little, *Morphogenesis of the first blood vessels*. Ann N Y Acad Sci, 1998. **857**: p. 155-79.
143. Hungerford, J.E. and C.D. Little, *Developmental biology of the vascular smooth muscle cell: building a multilayered vessel wall*. J Vasc Res, 1999. **36**(1): p. 2-27.
144. Martin, I., D. Wendt, and M. Heberer, *The role of bioreactors in tissue engineering*. Trends Biotechnol, 2004. **22**(2): p. 80-6.
145. O'Connell, M.K., et al., *The three-dimensional micro- and nanostructure of the aortic medial lamellar unit measured using 3D confocal and electron microscopy imaging*. Matrix Biol, 2008. **27**(3): p. 171-81.
146. C. Norotte, F.M.A.N.I.K.a.G.F., *Experimental evaluation of apparent tissue surface tension based on the exact solution of the Laplace equation*. EPL (Europhysics Letters), 2008. **81**(4): p. 46003.
147. Alobaid, N., et al., *Single stage cell seeding of small diameter prosthetic cardiovascular grafts*. Clin Hemorheol Microcirc, 2005. **33**(3): p. 209-26.
148. Sarkar, S., et al., *The mechanical properties of infrainguinal vascular bypass grafts: their role in influencing patency*. Eur J Vasc Endovasc Surg, 2006. **31**(6): p. 627-36.
149. Dahl, S.L., M.E. Vaughn, and L.E. Niklason, *An ultrastructural analysis of collagen in tissue engineered arteries*. Ann Biomed Eng, 2007. **35**(10): p. 1749-55.
150. Lareu, R.R., et al., *In vitro enhancement of collagen matrix formation and crosslinking for applications in tissue engineering: a preliminary study*. Tissue Eng, 2007. **13**(2): p. 385-91.

VITA

Cyrille Norotte was born in Paris, France in 1983. He graduated from Janson de Sailly High School, Paris, in 2000 with a scientific profile. He attended Medical School at Universite Rene Descartes, Paris, from 2000 to 2004. At the same time he was accepted in the M.D.- Ph.D. program of Inserm School in 2003, which led him to attend Graduate School at Universite Pierre et Marie Curie, Paris, where he received a Master of Science degree in Developmental Biology in 2005. He then enrolled in graduate school at the University of Missouri-Columbia to pursue a Ph.D. in Biological Sciences. In 2009, he will go back to Universite Rene Descartes, Paris, to complete his medical training.